

# Test of new physics effects in $\bar{B} \rightarrow (D^{(*)}, \pi)\ell^{-}\bar{\nu}_\ell$ decays with heavy and light leptons

Ipsita Ray<sup>1,2,\*</sup> and Soumitra Nandi<sup>1,†</sup>

<sup>1</sup>*Indian Institute of Technology, North Guwahati, Guwahati 781039, Assam, India*

<sup>2</sup>*Indian Institute of Technology Gandhinagar Palaj, Gandhinagar - 382055, Gujarat, India*

We study the  $\bar{B} \rightarrow D(D^{(*)})\ell^{-}\bar{\nu}_\ell$  decays based on the up-to-date available inputs from experiments and the lattice. First, we review the standard model (SM) predictions of the different observables associated with these decay channels. In the analyses, we consider new physics (NP) effects in the channels with the heavy ( $\tau$ ), as well as the light leptons ( $\mu, e$ ). We have extracted  $|V_{cb}|$  along with the new Wilson coefficients (WCs) from the available data on light leptons; the extracted value of  $|V_{cb}|$  is  $(40.3 \pm 0.5) \times 10^{-3}$ . The extracted WCs are zero consistent, but some could be of order  $10^{-2}$ . Also, we have done the simultaneous analysis of the data in  $\bar{B} \rightarrow D^{(*)}(\mu^{-}, e^{-})\bar{\nu}$  alongside the inputs on  $R(D^{(*)}) = \frac{\Gamma(\bar{B} \rightarrow D^{(*)}\tau^{-}\bar{\nu}_\tau)}{\Gamma(\bar{B} \rightarrow D^{(*)}\ell^{-}\bar{\nu}_\ell)}$  and the  $D^{*}$  longitudinal polarisation fraction  $F_L^{D^{*}}$  in different NP scenarios and extracted  $|V_{cb}|$  which is consistent with the number mentioned above. Also, the simultaneous explanation of  $R(D^{(*)})$  and  $F_L^{D^{*}}$  is not possible in the one-operator scenarios. However, the two operator scenarios with  $\mathcal{O}_{S_2}^\tau = (\bar{q}_R b_L)(\bar{\tau}_R \nu_{\tau L})$  as one of the operators could explain all these three measurements. Finally, we have given predictions of all the related observables in  $\bar{B} \rightarrow D^{(*)}(\tau^{-}, \mu^{-}, e^{-})\bar{\nu}$  decays in the NP scenarios, which could be tested in future experiments. We have repeated this exercise for  $\bar{B} \rightarrow \pi\ell^{-}\bar{\nu}_\ell$  decays with the light lepton and extracted  $|V_{ub}|$  and the new WCs. Finally, using all these available data for the light and heavy leptons, we have given bounds on the couplings of the relevant SM effective field theory (SMEFT) operators and the probable NP scale  $\Lambda$ .

## I. INTRODUCTION

For the last couple of years, special attention has been given to the flavour-changing neutral current (FCNC) and charged current (FCCC) semileptonic  $B$  and  $B_s$  decays. In this paper, we will focus on  $\bar{B} \rightarrow D(D^{(*)})\ell^{-}\bar{\nu}_\ell$  and  $\bar{B} \rightarrow \pi\ell^{-}\bar{\nu}_\ell$  decays, which are the FCCC semileptonic decays of  $B$  meson. Here, we can identify  $\ell$  as the light leptons like  $e$  and  $\mu$  or the heavy lepton  $\tau$ . The processes with the light leptons were assumed to be insensitive to any new physics effects, and the data on these modes are used to extract the CKM elements  $|V_{cb}|$  and  $|V_{ub}|$  from the  $\bar{B} \rightarrow D(D^{(*)})\ell^{-}\bar{\nu}_\ell$  and  $\bar{B} \rightarrow \pi\ell^{-}\bar{\nu}_\ell$  decays, respectively, for the updated analyses, see [1–12] and the references therein. Right now, alongside the experimental data on the differential rates [13–22], we have very precise inputs from the lattice on the respective form factors at zero and non-zero recoils [23–30]. With this wealth of data, it is possible to extract  $|V_{cb}|$  and  $|V_{ub}|$  and the possible new physics effects in  $b \rightarrow c\ell^{-}\bar{\nu}_\ell$  and  $b \rightarrow u\ell^{-}\bar{\nu}_\ell$  decays along with the respective parameters parametrising the form factors of the decays as mentioned above. In this paper, we have analysed all the available data and the lattice inputs on these modes, extracted the respective CKM elements, and constrained the model-independent new physics (NP) information alongside the shape of the form factors.

For the same decay modes we can define the ratio of the decays rates  $R(D^{(*)}) = \frac{\Gamma(\bar{B} \rightarrow D^{(*)}\tau^{-}\bar{\nu}_\tau)}{\Gamma(\bar{B} \rightarrow D^{(*)}\ell^{-}\bar{\nu}_\ell)}$ . These observables are potentially sensitive to lepton flavor universality violating (LFUV) new physics effects in these decays. At the moment, measurements are available on  $R(D)$  and  $R(D^{*})$ . The measured value of  $R(D)$  is given by [31, 32]

$$R(D) = 0.356 \pm 0.029 \quad (1)$$

which is the average of the measurements in the refs. [33–37]. There is disagreement between the measurement and the SM prediction  $R(D)_{SM} = 0.298 \pm 0.004$  [32] which is an arithmetic average of the estimates obtained in the refs. [7, 31, 38–41]. On the other hand, the measured value of  $R(D^{*})$  is given by

$$R(D^{*}) = 0.291 \pm 0.014, \quad (2)$$

which has been obtained from an average of the estimates in [33–37, 42]. Very recently, LHCb has announced their new result on  $R(D^{*})$  [43], which, when combined with their earlier measurement [44], the average will be

$$R(D^{*}) = 0.257 \pm 0.012 \pm 0.018. \quad (3)$$

\* ipsitaray02@gmail.com

† soumitra.nandi@iitg.ac.in

On combining this result with the average given in eq. 2, HFLAV has obtained the new average [32]

$$R(D^*) = 0.284 \pm 0.013. \quad (4)$$

The SM predictions for the  $R(D^*)_{SM} = 0.254 \pm 0.005$ , the arithmetic average of the predictions obtained in the refs. [1, 2, 32, 39–41, 45]. Apart from [45], the rest of the analyses are based on the data from Belle [14, 15], and one input on the form factor from the lattice at zero recoil has been considered [25]. As a recent update, the Fermilab-MILC collaboration estimated the form factors for  $\bar{B} \rightarrow D^* \ell^- \bar{\nu}_\ell$  decays at the non-zero recoils utilising which they have obtained  $R(D^*)_{SM} = 0.265 \pm 0.013$ . This estimate does not include the input from the experimental measurements. It is completely based on the lattice inputs and consistent with the measurement presented in eq. 4. Note that the SM prediction (only lattice) and the measurement have large errors. In the case of  $R(D)$ , the measurement has a large error compared to the corresponding SM estimate. We have to wait for more precise inputs from the lattice and more precise data from the experimental measurements. It is important to note that the data on  $\bar{B} \rightarrow D(D^*) \ell^- \bar{\nu}_\ell$  with light lepton are useful to constrain the shape of the form factors on top of the lattice data. However, doing the fits in the presence of NP contributions in these modes will be more appropriate. Therefore, the present data could be useful to constrain the new physics contributions in  $b \rightarrow c \ell^- \bar{\nu}_\ell$  and  $b \rightarrow c \tau^- \bar{\nu}_\tau$  decays alongside the extraction of  $|V_{cb}|$  which is our main focus in this paper. In principle, the NP contributions in  $b \rightarrow c \ell^- \bar{\nu}_\ell$  and  $b \rightarrow c \tau^- \bar{\nu}_\tau$  could be different or they could be of similar nature, we have explored both these possibilities and constrained the new model-independent Wilson coefficients.

In addition to the  $R(D)$  and  $R(D^*)$ , measurements are available on the  $\tau$  polarization asymmetry  $P_\tau^{D^*}$  [42] and the  $D^*$  longitudinal polarization fraction  $F_L(D^*)$  [46]. The respective estimates are the following

$$P_\tau^{D^*} = -0.38 \pm 0.51(stat)_{-0.16}^{+0.21}(sys), \quad F_L^{D^*} = 0.60 \pm 0.08(stat) \pm 0.04(sys). \quad (5)$$

Note that the measurement for the  $\tau$  polarization has an error of more than 100%, and the measurement of  $F_L^{D^*}$  is not a published article. The SM predictions can be seen from [2], which were based on the Belle 2017 and/or 2019 results, and by then, available inputs on the respective form factors in  $B \rightarrow D^*$  decays at zero recoil. In this paper we will update those numbers. Also, we will update the SM predictions of the relevant observables in  $\bar{B} \rightarrow D \ell^- \bar{\nu}_\ell$  decays, for the older results one could see the ref. [47, 48]. We haven't considered  $P_\tau(D^*)$  as input in our analysis. However, we have checked that the predictions are not exceeding the experimental limits. In a few fits, we have included  $F_L(D^*)$  to check the impact of this measurement.

The Effective field theory (EFT) is an important framework to deal with phenomenon that are spread over a multitude of energy or length scales, such as the electroweak scale determining flavor-changing transitions of quarks and the scale of strong interactions related to the formation of hadrons. Hence, the low energy data could be useful to constrain the scale of the new physics. In the framework of the SM Effective Field Theory (SMEFT), the renormalizable dimension-4 SM Lagrangian is extended by higher dimensional operators suppressed by powers of the new physics scale  $\Lambda$  [49].

$$\mathcal{L}_{\text{eff}} = \mathcal{L}_{\text{SM}} + \sum_i \frac{1}{\Lambda^{d_i-4}} C_i \mathcal{O}_i \quad (6)$$

where  $\Lambda$  is the cutoff scale of the EFT,  $\mathcal{O}_i$  are a set of dimension  $d_i$  operators that are invariant under the  $SU(3)_c \times SU(2)_L \times U(1)_Y$  gauge group and  $C_i$  are their respective Wilson coefficients (WC). New physics at higher energy scales is encoded in the Wilson coefficients of higher dimensional operators. The WCs of the low energy effective operators could be obtained by matching the SMEFT to these operators and following an appropriate renormalization group evolution equations (RGE) [50, 51]. In this analysis, we have obtained the constraints on the ratio  $\frac{C_i}{\Lambda^2}$  from the available data on the exclusive  $\bar{B} \rightarrow (D, D^*, \pi) \ell^- \bar{\nu}_\ell$  decays. These decays can be described by writing down the most general dimension-6 operators, which we will discuss in the next section.

## II. FRAMEWORK

Assuming the neutrinos to be left-handed, the most general effective Hamiltonian with all possible four-fermion operators relevant for  $b \rightarrow c(u) \ell^- \bar{\nu}_\ell$  is given as [52]

$$\mathcal{H}_{\text{eff}}^{b \rightarrow q \ell^- \bar{\nu}_\ell} = \frac{4G_F}{\sqrt{2}} V_{qb} [(1 + C_{V_1}^l) \mathcal{O}_{V_1}^l + C_{V_2}^l \mathcal{O}_{V_2}^l + C_{S_1}^l \mathcal{O}_{S_1}^l + C_{S_2}^l \mathcal{O}_{S_2}^l + C_T^l \mathcal{O}_T^l] \quad (7)$$

where the four-Fermi operators are given by,

$$\begin{aligned}
\mathcal{O}_{V_1}^l &= (\bar{q}_L \gamma^\mu b_L)(\bar{l}_L \gamma_\mu \nu_{lL}), \\
\mathcal{O}_{V_2}^l &= (\bar{q}_R \gamma^\mu b_R)(\bar{l}_L \gamma_\mu \nu_{lL}), \\
\mathcal{O}_{S_1}^l &= (\bar{q}_L b_R)(\bar{l}_R \nu_{lL}), \\
\mathcal{O}_{S_2}^l &= (\bar{q}_R b_L)(\bar{l}_R \nu_{lL}), \\
\mathcal{O}_T^l &= (\bar{q}_R \sigma^{\mu\nu} b_L)(\bar{l}_R \sigma_{\mu\nu} \nu_{lL}),
\end{aligned} \tag{8}$$

with  $q = u$  or  $c$ . In the Standard Model, the WC  $C_i^\ell = 0$ , hence the WCs defined in eq. 7 are associated only with the new operators beyond the SM. We will constrain these WCs from the available data. Using the available experimental data on the  $\bar{B} \rightarrow D(D^*)\ell^-\bar{\nu}_\ell$ ,  $R(D^{(*)})$ ,  $\bar{B} \rightarrow \pi\ell^-\bar{\nu}_\ell$  ( $\ell = \mu, e$ ) and the available lattice inputs, we can extract these WCs. In this analysis, we have considered only the real WCs.

In the SMEFT, the operators which will be relevant for the  $b \rightarrow c(u)\ell^-\bar{\nu}_\ell$  transitions are given by [51]

$$\begin{aligned}
Q_{\ell q}^{(3)} &= (\bar{\ell}_i \gamma_\mu \tau^I \ell_j)(\bar{q}_k \gamma^\mu \tau^I q_l), & Q_{\phi ud} &= i(\tilde{\phi}^\dagger D_\mu \phi)(\bar{u}_i \gamma^\mu d_j), \\
Q_{\ell edq} &= (\bar{\ell}_i^a e_j)(\bar{d}_k q_l^a), & Q_{\ell equ}^{(1)} &= (\bar{\ell}_i^a e_j)\epsilon_{ab}(\bar{q}_k^b u_l), \\
Q_{\ell equ}^{(3)} &= (\bar{\ell}_i^a \sigma^{\mu\nu} e_j)\epsilon_{ab}(\bar{q}_k^b \sigma_{\mu\nu} u_l), & Q_{\phi q}^{(3)} &= (\phi^\dagger i\overleftrightarrow{D}_\mu \phi)(\bar{q}_i \tau^I \gamma^\mu q_j)
\end{aligned} \tag{9}$$

In the above equation,  $\ell, q$  and  $\phi$  represent lepton, quark and Higgs  $SU(2)_L$  doublets, while the right-handed isospin singlets are denoted by  $e, u$  and  $d$ .

By matching these Standard Model gauge invariant dimension-six operators at the electroweak scale onto the low-energy  $B$  physics Hamiltonian by integrating out the top quark,  $Z$  and  $W$  bosons and the Higgs boson, the Wilson coefficients (WCs) are obtained [51]. These WCs are then evolved from the electroweak scale  $\mu_W$  to the scale  $\mu_b$  relevant to  $B$  physics measurements by the appropriate RGE equations. As a result, the WCs of the operators defined in eq. 7 are obtained as a linear combination of the Wilson coefficients of the corresponding operators of the SMEFT basis. Thus, the low-energy experiments in flavour physics can be used to constrain these coefficients of the SMEFT operator basis.

Following the method discussed above, a tree-level matching of the SMEFT operators (eq. 9) to the effective operator basis defined in eqs. 7 and 8 will result in the following WCs at the scale  $m_b$  for  $b \rightarrow c\ell^-\bar{\nu}_\ell$  decays [51]

$$\begin{aligned}
C_{V_1} &= -\frac{v^2}{\Lambda^2} \frac{V_{cs}}{V_{cb}} (\tilde{C}_{\ell q}^{(3)ll23} - \tilde{C}_{\phi q}^{(3)23}), & C_{V_2} &= \frac{v^2}{2\Lambda^2 V_{cb}} \tilde{C}_{\phi ud}^{23}, \\
C_{S_1} &= -\frac{v^2}{2\Lambda^2} \frac{V_{cs}}{V_{cb}} \tilde{C}_{\ell edq}^{*ll32}, & C_{S_2} &= -\frac{v^2}{2\Lambda^2} \frac{V_{tb}}{V_{cb}} \tilde{C}_{\ell equ}^{*(1)ll32}, \\
C_T &= -\frac{v^2}{2\Lambda^2} \frac{V_{tb}}{V_{cb}} \tilde{C}_{\ell equ}^{*(3)ll32}
\end{aligned} \tag{10}$$

and that for  $b \rightarrow u\ell^-\bar{\nu}_\ell$  transitions,

$$\begin{aligned}
C_{V_1} &= -\frac{v^2}{\Lambda^2} \frac{V_{ud}}{V_{ub}} (\tilde{C}_{\ell q}^{(3)ll13} - \tilde{C}_{\phi q}^{(3)13}), & C_{V_2} &= \frac{v^2}{2\Lambda^2 V_{ub}} \tilde{C}_{\phi ud}^{13}, \\
C_{S_1} &= -\frac{v^2}{2\Lambda^2} \frac{V_{ud}}{V_{ub}} \tilde{C}_{\ell edq}^{*ll31}, & C_{S_2} &= -\frac{v^2}{2\Lambda^2} \frac{V_{tb}}{V_{ub}} \tilde{C}_{\ell equ}^{*(1)ll31}, \\
C_T &= -\frac{v^2}{2\Lambda^2} \frac{V_{tb}}{V_{ub}} \tilde{C}_{\ell equ}^{*(3)ll31}
\end{aligned} \tag{11}$$

From hereon, we will denote  $(\tilde{C}_{\ell q}^{(3)ll23} - \tilde{C}_{\phi q}^{(3)23}) = \tilde{C}_{\ell q}^{(3)}$  since we can only constrain the difference from the fits. Here,  $v$  is the Higgs vacuum expectation value, and  $\Lambda$  is the new physics scale. In eqs. 10 and 11, we have neglected the sub-dominant CKM elements. Here, the  $\tilde{C}$ s are the WCs or the couplings of the respective SMEFT operators at the electroweak scale  $\mu_{EW}$ . We will use the available experimental results on the  $\bar{B} \rightarrow D(D^*)\ell^-\bar{\nu}_\ell$ ,  $\bar{B} \rightarrow \pi\ell^-\bar{\nu}_\ell$  and  $R(D^{(*)})$  alongside the lattice inputs mentioned in the introduction to fit the ratios  $\tilde{C}/\Lambda^2$  given in the above equations. The result will help us to pinpoint the scale of new physics  $\Lambda$  for particular choices of the couplings or vice versa. We will discuss this in detail in the following sections.

Constants	Values
$G_F$	$1.166 \times 10^{-5} \text{ GeV}^{-2}$
$\chi_{1-}^T(0)$ (for $g$ and $f_+$ )	$5.131 \times 10^{-4} \text{ GeV}^{-2}$
$\chi_{1+}^T(0)$ (for $f$ and $F_1$ )	$3.894 \times 10^{-4} \text{ GeV}^{-2}$
$\chi_{0-}^L(0)$ (for $F_2$ )	$1.9421 \times 10^{-2} \text{ GeV}^{-2}$
$\chi_{0+}^L(0)$ (for $f_0$ )	$6.204 \times 10^{-3} \text{ GeV}^{-2}$

TABLE I: Various inputs used in this analysis [53].

Form factor involved	$B_c^{(*)}$ pole masses (GeV)
$f_+$ and $g$	6.32847, 6.91947, 7.030
$f$ and $F_1$	6.73847, 6.750, 7.145, 7.150
$F_2$	6.27447, 6.8712, 7.250
$f_0$	6.70347, 7.122

TABLE II: Pole masses used in the  $B \rightarrow D^{(*)}$  modes.

### A. $\bar{B} \rightarrow D(\pi)\ell^- \bar{\nu}_\ell$

Using the above effective Hamiltonian, the differential decay rate in the presence of new physics for  $\bar{B} \rightarrow D\ell^- \bar{\nu}$  transitions can be written as [52] (both for heavy and light leptons):

$$\begin{aligned}
\frac{d\Gamma(\bar{B} \rightarrow D\ell^- \bar{\nu}_\ell)}{dq^2} &= \frac{G_F^2 \eta_{EW}^2 |V_{cb}|^2}{192\pi^3 m_B^3} q^2 \sqrt{\lambda_D(q^2)} \left(1 - \frac{m_\ell^2}{q^2}\right)^2 \times \left\{ |1 + C_{V_1}^l + C_{V_2}^l|^2 \left[ \left(1 + \frac{m_\ell^2}{2q^2}\right) H_{V,0}^{s,2} + \frac{3}{2} \frac{m_\ell^2}{q^2} H_{V,t}^{s,2} \right] \right. \\
&\quad + \frac{3}{2} |C_{S_1}^l + C_{S_2}^l|^2 H_S^{s,2} + 8|C_T^l|^2 \left(1 + \frac{2m_\ell^2}{q^2}\right) H_T^{s,2} + 3\text{Re}[(1 + C_{V_1}^l + C_{V_2}^l)(C_{S_1}^{l*} + C_{S_2}^{l*})] \\
&\quad \left. \frac{m_\ell}{\sqrt{q^2}} H_S^s H_{V,t}^s - 12\text{Re}[(1 + C_{V_1}^l + C_{V_2}^l)C_T^{l*}] \frac{m_\ell}{\sqrt{q^2}} H_T^s H_{V,0}^s \right\}, \tag{12}
\end{aligned}$$

where  $\lambda_D(q^2) = ((m_B - m_D)^2 - q^2)((m_B + m_D)^2 - q^2)$  and

$$\begin{aligned}
H_{V,0}^s(q^2) &= \sqrt{\frac{\lambda_D(q^2)}{q^2}} f_+(q^2), & H_{V,t}^s(q^2) &= \frac{m_B^2 - m_D^2}{\sqrt{q^2}} f_0(q^2) \\
H_S^s(q^2) &= \frac{m_B^2 - m_D^2}{m_b - m_c} f_0(q^2), & H_T^s(q^2) &= -\frac{\sqrt{\lambda_D(q^2)}}{m_B + m_D} f_T(q^2)
\end{aligned} \tag{13}$$

The form factors are expanded in the BGL method of parametrization as [54]

$$\mathcal{F}_i(z) = \frac{1}{P_i(z)\phi_i(z)} \sum_{j=0}^N a_j^i z^j, \tag{14}$$

where  $z$  is related to the recoil variable  $w$  as

$$z = \frac{\sqrt{w+1} - \sqrt{2}}{\sqrt{w+1} + \sqrt{2}}. \tag{15}$$

$w$  is related to the momentum transferred to the dilepton system ( $q^2$ ) as  $q^2 = m_B^2 + m_f^2 - 2m_B m_f w$ .

The functions  $P_i(z)$ , called the Blaschke factors, are given by

$$P_i(z) = \prod_p \frac{z - z_p}{1 - zz_p}, \quad (16)$$

which are used to eliminate the poles at  $z = z_p$  where,

$$z_p = \frac{\sqrt{(m_B + m_f)^2 - m_P^2} - \sqrt{4m_B m_f}}{\sqrt{(m_B + m_f)^2 - m_P^2} + \sqrt{4m_B m_f}}. \quad (17)$$

Here  $m_P$  denotes the pole masses, details in [53]. The outer functions  $\phi_i(z)$  can be any analytic function of  $q^2$  and are chosen to be [55]

$$\begin{aligned} \phi_{f_+} &= \frac{8r^2}{m_B} \sqrt{\frac{8n_I}{3\pi\tilde{\chi}_{1-}^T(0)}} \frac{(1+z)^2(1-z)^{1/2}}{[(1+r)(1-z) + 2\sqrt{r}(1+z)]^5}, \\ \phi_{f_0} &= r(1-r^2) \sqrt{\frac{8n_I}{\pi\tilde{\chi}_{1-}^L(0)}} \frac{(1-z^2)(1-z)^{1/2}}{[(1+r)(1-z) + 2\sqrt{r}(1+z)]^4}, \end{aligned} \quad (18)$$

where  $r = m_D/m_B$ .

If we write the double-differential decay distribution as [56]

$$\frac{d^2\Gamma_l}{dq^2 d\cos\theta} = a_l(q^2) + b_l(q^2) \cos\theta + c_l(q^2) \cos^2\theta, \quad (19)$$

where  $\theta$  is the polar angle of the lepton momentum in the rest frame of the  $l\bar{\nu}$  pair with respect to the  $z$  axis which is defined by the  $D$ -momentum in the rest frame of  $\bar{B}$ , the lepton forward-backward asymmetry is defined as

$$A_{FB}(q^2) = \frac{\int_0^1 \frac{d^2\Gamma}{dq^2 d\cos\theta_l} d\cos\theta_l - \int_{-1}^0 \frac{d^2\Gamma}{dq^2 d\cos\theta_l} d\cos\theta_l}{d\Gamma/dq^2} = \frac{b_l(q^2)}{d\Gamma/dq^2} \quad (20)$$

and the lepton polarization asymmetry is defined as

$$A_{\lambda_l}^D(q^2) = -P_\ell^D = \frac{d\Gamma^{\lambda_l=-1/2}/dq^2 - d\Gamma^{\lambda_l=+1/2}/dq^2}{d\Gamma/dq^2}. \quad (21)$$

Note that the our definition for the lepton polarization asymmetry has a sign difference with respect to the one used by Belle (eq. 5).

The rate for the  $\bar{B} \rightarrow \pi\ell^-\bar{\nu}_\ell$  decays are similar to the one given in eq. 12 with the inputs for the  $D$  meson replaced by that for the pions. To get the shape of the decay rate, we need to determine the shape of the form factors for  $\bar{B} \rightarrow \pi\ell^-\bar{\nu}_\ell$ . For the form factors, we use the simplified series expansion in  $z$  as given in ref. [57] by Bharucha-Straub-Zwicky (BSZ):

$$f_i(q^2) = \frac{1}{1 - q^2/m_{R,i}^2} \sum_{k=0}^N a_k^i [z(q^2; t_0) - z(0; t_0)]^k, \quad (22)$$

where  $z$  is defined as before in eqs. 15 and 17, respectively. In eq 22,  $m_{R,i}$  denotes the mass of the sub-threshold resonances compatible with the quantum numbers of the respective form factors and  $a_k^i$ s are the coefficients of expansion, the details are given in ref [57]. Another commonly used approach for the parametrizations of the  $B \rightarrow \pi$  form factors in the literature is provided by Bourrely-Caprini-Lellouch (BCL) [58]. A comparative study of these two approaches in the extractions of  $|V_{ub}|$  from  $\bar{B} \rightarrow \pi\ell^-\bar{\nu}_\ell$  decays has been undertaken in ref. [4]. The results are extremely consistent with each other in both approaches. For interested readers, a more detailed discussion on this topic could also be seen from our earlier paper [12].

Observables	Lattice		Lattice combined	Lattice [23, 24]	Lattice [23, 24]	Lattice [23, 24, 28, 30]
	MILC [28]	JLQCD [30]	$B \rightarrow D$ [23, 24] $B \rightarrow D^*$ [28, 30]	[28, 30] + Expt [13, 15, 16]	[28, 30] + LCSR ( $q^2 = 0$ )[59]	+ LCSR ( $q^2 = 0$ ) [59] + Expt [13, 15, 16]
$R(D)$			0.304(3)	0.300(3)	0.304(3)	0.300(3)
$R(D^*)$	0.271(31)	0.253(22)	0.258(12)	0.251(1)	0.253(9)	0.251(1)
$F_L^{\bar{B} \rightarrow D^* \tau^- \bar{\nu}}$	0.422(11)	0.446(22)	0.427(9)	0.453(3)	0.439(6)	0.453(3)
$A_{\lambda_\tau}^{D^*} = -P_\tau^{D^*}$	0.526(11)	0.509(15)	0.519(7)	0.507(3)	0.512(5)	0.506(3)
$A_{FB}^{\bar{B} \rightarrow D^* \tau^- \bar{\nu}}$	-0.082(12)	-0.053(21)	-0.077(9)	-0.051(4)	-0.070(7)	-0.051(4)
$A_{\lambda_\tau}^D = -P_\tau^D$			-0.324(3)	-0.323(3)	-0.324(3)	-0.323(3)
$A_{FB}^{\bar{B} \rightarrow D \tau^- \bar{\nu}}$			0.3596(4)	0.3600(2)	0.3596(4)	0.3600(2)
$A_{\lambda_\mu}^{D^*} = -P_\mu^{D^*}$	0.989(4)	0.986(4)	0.987(2)	0.9852(2)	0.986(1)	0.9852(2)
$F_L^{\bar{B} \rightarrow D^* \mu^- \bar{\nu}}$	0.463(36)	0.510(60)	0.480(22)	0.530(3)	0.506(15)	0.530(3)
$A_{FB}^{\bar{B} \rightarrow D^* \mu^- \bar{\nu}}$	-0.247(29)	-0.215(35)	-0.243(17)	-0.208(3)	-0.233(11)	-0.209(3)
$A_{\lambda_\mu}^D = -P_\mu^D$			0.9618(2)	0.9615(2)	0.9618(2)	0.9615(2)
$A_{FB}^{\bar{B} \rightarrow D \mu^- \bar{\nu}}$			0.01369(10)	0.01380(8)	0.01369(10)	0.01379(8)
$F_L^{\bar{B} \rightarrow D^* e^- \bar{\nu}}$	0.463(36)	0.510(60)	0.480(23)	0.530(3)	0.507(15)	0.530(3)
$A_{FB}^{\bar{B} \rightarrow D^* e^- \bar{\nu}}$	-0.250(29)	-0.220(34)	-0.247(17)	-0.214(3)	-0.238(10)	-0.214(3)

TABLE III: Predictions of the observables in the  $B \rightarrow D^{(*)}$  channel in different scenarios. Here, the experimental data is in the  $\bar{B} \rightarrow D(\mu, e)\bar{\nu}$  and  $\bar{B} \rightarrow D^*(\mu, e)\bar{\nu}$  decays.

### B. $\bar{B} \rightarrow D^* l^- \bar{\nu}$

The decay distribution for the four body decay  $\bar{B} \rightarrow D^*(\rightarrow D\pi)l^- \bar{\nu}_l$  can be completely described in terms of four kinematic variables: the lepton invariant mass squared ( $q^2$ ) and the three angles [56]

$$\frac{d^4\Gamma}{dq^2 d\cos\theta_l d\cos\theta_V d\phi} = \frac{9}{32\pi} I(q^2, \theta_l, \theta_V, \phi) \quad (23)$$

where,

$$\begin{aligned} I(q^2, \theta_l, \theta_V, \phi) = & I_1^s \sin^2\theta_V + I_1^c \cos^2\theta_V + (I_2^s \sin^2\theta_V + I_2^c \cos^2\theta_V) \cos 2\theta_l + I_3 \sin^2\theta_V \sin^2\theta_l \cos 2\phi \\ & + I_4 \sin 2\theta_V \sin 2\theta_l \cos \phi + I_5 \sin 2\theta_V \sin \theta_l \cos \phi + (I_6^s \sin^2\theta_V + I_6^c \cos^2\theta_V) \cos \theta_l \\ & + I_7 \sin 2\theta_V \sin \theta_l \sin \phi + I_8 \sin 2\theta_V \sin 2\theta_l \sin \phi + I_9 \sin^2\theta_V \sin^2\theta_l \sin 2\phi \end{aligned} \quad (24)$$

The angular coefficients ( $I$ 's) are written in terms of the helicity amplitudes  $H_\lambda$  as well as their linear combinations [56] which are in turn expressed as functions of the form factors ( $f, g, F_1, F_2$ ) in the BGL basis and the Wilson coefficients. The outer functions with  $r = m_{D^*}/m_B$  are expressed as [55]

$$\begin{aligned} \phi_f &= \frac{4r}{m_B^2} \sqrt{\frac{n_I}{6\pi\tilde{\chi}_{1+}^T(0)}} \frac{(1+z)(1-z)^{3/2}}{[(1+r)(1-z) + 2\sqrt{r}(1+z)]^4}, \\ \phi_g &= 16r^2 \sqrt{\frac{n_I}{3\pi\tilde{\chi}_{1-}^T(0)}} \frac{(1+z)^2(1-z)^{-1/2}}{[(1+r)(1-z) + 2\sqrt{r}(1+z)]^4}, \\ \phi_{\mathcal{F}_1} &= \frac{4r}{m_B^3} \sqrt{\frac{n_I}{6\pi\chi_{1+}^T(0)}} \frac{(1+z)(1-z)^{5/2}}{[(1+r)(1-z) + 2\sqrt{r}(1+z)]^5}, \\ \phi_{\mathcal{F}_2} &= 8\sqrt{2}r^2 \sqrt{\frac{n_I}{\pi\tilde{\chi}_{1+}^L(0)}} \frac{(1+z)^2(1-z)^{-1/2}}{[(1+r)(1-z) + 2\sqrt{r}(1+z)]^4} \end{aligned} \quad (25)$$

Scenario	From the simultaneous fit to all unknowns		BGL coefficients are nuisance parameters	
	Fit Parameters	Predictions	Fit Parameters	Predictions
$C_{V_2}$	$C_{V_2} = -0.005 \pm 0.014$ $ V_{cb}  = (40.2 \pm 0.6) \times 10^{-3}$	$R(D) = 0.300 \pm 0.003,$ $R(D^*) = 0.251 \pm 0.001$	$C_{V_2} = 0.003 \pm 0.015$ $ V_{cb}  = (40.5 \pm 0.6) \times 10^{-3}$	$R(D) = 0.298 \pm 0.005,$ $R(D^*) = 0.251 \pm 0.002$
$C_T$	$C_T = (0.2 \pm 4.9) \times 10^{-4}$ $ V_{cb}  = (40.3 \pm 0.5) \times 10^{-3}$	$R(D) = 0.300 \pm 0.003,$ $R(D^*) = 0.251 \pm 0.001$	$C_T = (0.4 \pm 5.0) \times 10^{-4}$ $ V_{cb}  = (40.5 \pm 0.5) \times 10^{-3}$	$R(D) = 0.298 \pm 0.005,$ $R(D^*) = 0.251 \pm 0.001$
$C_{S_1}$	$C_{S_1} = (-0.003 \pm 0.046)$ $ V_{cb}  = (40.3 \pm 0.5) \times 10^{-3}$	$R(D) = 0.299 \pm 0.022,$ $R(D^*) = 0.251 \pm 0.002$	$C_{S_1} = (-0.005 \pm 0.047)$ $ V_{cb}  = (40.5 \pm 0.5) \times 10^{-3}$	$R(D) = 0.295 \pm 0.022,$ $R(D^*) = 0.251 \pm 0.002$
$C_{S_2}$	$C_{S_2} = -0.002 \pm 0.046$ $ V_{cb}  = (40.3 \pm 0.5) \times 10^{-3}$	$R(D) = 0.299 \pm 0.021,$ $R(D^*) = 0.251 \pm 0.002$	$C_{S_2} = 0.0001 \pm 0.0464$ $ V_{cb}  = (40.5 \pm 0.5) \times 10^{-3}$	$R(D) = 0.298 \pm 0.022,$ $R(D^*) = 0.251 \pm 0.002$

TABLE IV: The simultaneous fit of  $|V_{cb}|$  and the new WCs. The inputs are the ‘‘Lattice + LCSR( $q^2 = 0$ ) + data on  $\bar{B} \rightarrow D(\mu, e)\bar{\nu}$  and  $\bar{B} \rightarrow D^*(\mu, e)\bar{\nu}$  decays’’. The fit results for the BGL coefficients are given in a separate file. The predictions of  $R(D)$  and  $R(D^*)$  using the fit results in different scenarios are also shown.

In table I, we give the values of the susceptibilities  $\chi$  relevant to the different form factors. The pole masses used in  $B \rightarrow D^{(*)}$  channel are given in table II.

For this mode, the various observables are defined as follows [56] :

$$A_{FB}(q^2) = \frac{3}{8} \frac{(I_6^c + 2I_6^s)}{d\Gamma/dq^2}, \quad (26a)$$

$$A_{\lambda_l}^{D^*}(q^2) = -P_\ell^{D^*} = \frac{d\Gamma^{\lambda_l=-1/2}/dq^2 - d\Gamma^{\lambda_l=+1/2}/dq^2}{d\Gamma/dq^2}, \quad (26b)$$

$$F_L^{D^*}(q^2) = \frac{3I_1^c - I_2^c}{3I_1^c + 6I_1^s - I_2^c - 2I_2^s}. \quad (26c)$$

As defined before,  $A_{FB}(q^2)$  and  $A_{\lambda_l}^{D^*}(q^2)$  are the forward backward asymmetry and the  $\tau$  polarization asymmetry, respectively. In addition, in this channel we have the longitudinal polarization fraction of  $D^*$  which is defined by  $F_L^{D^*}$ .

### III. ANALYSIS AND RESULTS

#### A. Inputs

In ref. [13], the Belle collaboration had analyzed the  $\bar{B} \rightarrow Dl^-\bar{\nu}$  decay. They provided measurements for the differential decay width in the recoil variable  $w$  in 10  $w$ -bins for both the charged and neutral  $B$  decays with electrons and muons in the final state. In 2018 and 2023, it presented the results for the differential distributions in  $w$ ,  $\cos\theta_l$ ,  $\cos\theta_\nu$  and  $\chi$  in 10 bins for the  $\bar{B} \rightarrow D^*l^-\bar{\nu}$  decay mode [15, 16]. For  $R(D^{(*)})$ , we consider the averages as performed by HFLAV [31, 32], the averages are obtained with and without the input on the very recent measurements on  $R(D^*)$  given in eq. 3. As mentioned in the introduction, in a few fits we have included the experimental data on  $F_L^{D^*}$  as input. In addition to these experimental results, we consider the inputs for the hadronic form factors available from various sources. For the  $B \rightarrow D$  form factors, we take lattice inputs from the Fermilab-MILC collaboration [23] and the HPQCD collaboration [24]. In [23], the form factors  $f_+$  and  $f_0$  are given at three values of the recoil variable  $w = 1, 1.08$  and  $1.16$ , whereas in [24], the fit results for the form factor parameters following BCL expansion are provided, using which we created synthetic data-points for  $f_+$  and  $f_0$  at  $w = 1, 1.06$  and  $1.12$  as their results are directly calculated for  $w \lesssim 1.12$ . The lattice inputs for the form factors of  $B \rightarrow D^*$  mode are taken from the Fermilab-MILC and JLQCD collaborations [28, 30] where the values of the form factors  $g, f, F_1$  and  $F_2$  are provided at non-zero values of the recoil parameter, namely  $w = 1.03, 1.10$  and  $1.17$  and  $w = 1.025, 1.06$  and  $1.10$  respectively. The lattice predictions are more reliable for the high- $q^2$  or low- $w$  values. In a couple of fits, we have also included the input on the form factors at  $q^2 = 0$  GeV<sup>2</sup> obtained from the Light Cone Sum Rule (LCSR) approach [59].

Scenario	From the simultaneous fit to all unknowns		BGL coefficients are nuisance parameters	
	Fit Parameters	Predictions	Fit Parameters	Predictions
$C_{V_2}$	$C_{V_2} = -0.005 \pm 0.014$ $ V_{cb}  = (40.3 \pm 0.6) \times 10^{-3}$	$R(D) = 0.301 \pm 0.003,$ $R(D^*) = 0.252 \pm 0.001$	$C_{V_2} = -0.004 \pm 0.014$ $ V_{cb}  = (40.3 \pm 0.6) \times 10^{-3}$	$R(D) = 0.301 \pm 0.003,$ $R(D^*) = 0.252 \pm 0.001$
$C_T$	$C_T = (-0.2 \pm 4.8) \times 10^{-4}$ $ V_{cb}  = (40.4 \pm 0.5) \times 10^{-3}$	$R(D) = 0.301 \pm 0.003,$ $R(D^*) = 0.252 \pm 0.001$	$C_T = (-0.2 \pm 4.9) \times 10^{-4}$ $ V_{cb}  = (40.4 \pm 0.5) \times 10^{-3}$	$R(D) = 0.301 \pm 0.003,$ $R(D^*) = 0.252 \pm 0.001$
$C_{S_1}$	$C_{S_1} = 0.06 \pm 0.03$ $ V_{cb}  = (40.3 \pm 0.5) \times 10^{-3}$	$R(D) = 0.326 \pm 0.012,$ $R(D^*) = 0.253 \pm 0.001$	$C_{S_1} = 0.06 \pm 0.03$ $ V_{cb}  = (40.3 \pm 0.5) \times 10^{-3}$	$R(D) = 0.325 \pm 0.012,$ $R(D^*) = 0.253 \pm 0.001$
$C_{S_2}$	$C_{S_2} = 0.05 \pm 0.03$ $ V_{cb}  = (40.3 \pm 0.6) \times 10^{-3}$	$R(D) = 0.322 \pm 0.013,$ $R(D^*) = 0.250 \pm 0.001$	$C_{S_2} = 0.05 \pm 0.03$ $ V_{cb}  = (40.3 \pm 0.5) \times 10^{-3}$	$R(D) = 0.322 \pm 0.013,$ $R(D^*) = 0.250 \pm 0.001$

TABLE V: The simultaneous fit of  $|V_{cb}|$  and the new WCs. The inputs are ‘‘Lattice + LCSR( $q^2 = 0$ ) + data on  $\bar{B} \rightarrow D(\mu, e)\bar{\nu}$  and  $\bar{B} \rightarrow D^*(\mu, e)\bar{\nu}$  decays +  $R(D^*)$ ’’. These fits assume similar NP in  $\tau$ ,  $\mu$  and  $e$  final states. Also, we have presented the values obtained on  $R(D^*)$  from the fit.

Data on the differential  $\bar{B} \rightarrow \pi l^- \bar{\nu}$  decay rates is available from BaBar (2011) [17], Belle (2011) [18], BaBar (2012) [21], Belle (2013) [22]. The lattice collaborations RBC/UKQCD [27] and JLQCD [29] provide synthetic data points for  $f_{+,0}(q^2)$  with full covariance matrices (both systematic and statistical) at three  $q^2$  points which we have directly used in our analysis. On the other hand, the Fermilab/MILC collaboration [26, 27] provides the fit results for the BCL coefficients of the  $z$ -expansions of the respective form factors. We use their fit results to generate correlated synthetic data points at the same  $q^2$  values as RBC/UKQCD, with an extra point for  $f_+$  at  $q^2 = 20.5 \text{ GeV}^2$ . In addition to the lattice inputs, we have used the inputs on the form factors  $f_+(q^2 = 0) = f_0(q^2 = 0)$  obtained by LCSR approaches [3] though the results are insensitive to this input.

Our first objective is to predict the observables  $R(D)$ ,  $R(D^*)$ ,  $A_{\lambda_\ell}^{D^{(*)}}$ ,  $A_{FB}^{D^{(*)}}$  and  $F_L^{D^*}$  in the SM for  $\bar{B} \rightarrow D^{(*)}\tau^- \bar{\nu}$ ,  $\bar{B} \rightarrow D^{(*)}\mu^- \bar{\nu}$  and  $\bar{B} \rightarrow D^{(*)}e^- \bar{\nu}$  decays. It is natural to expect that the experimental data could introduce bias in the SM predictions since the fit usually assumes no NP presence. To understand the gravity of impact, we have done these analyses in scenarios with and without the inputs from the experimental measurements on the decay rates in small  $q^2$  or angular bins for the light leptons like muons or electrons. Also, we have checked the impact of lattice and LCSR inputs. In table III, we have predicted these observables in six different analyses depending on the inputs used, which includes a comparative study of the predicted observables in the  $\bar{B} \rightarrow D^* l \bar{\nu}$  mode using the lattice inputs from Fermilab-MILC [28] and JLQCD [30] collaborations. Given the large errors, the respective Fermilab-MILC and JLQCD predictions are consistent at their  $1\sigma$  confidence interval (CI). The predictions of  $R(D)$  are consistent in all four scenarios defined in table III, so are the  $A_{FB}^{\bar{B} \rightarrow D^* \tau^- \bar{\nu}}$  and  $A_{\lambda_\tau}^D$ , due to the lattice’s precise inputs. Whether or not the experimental data are used, the predictions are very much consistent with each other. Also, we note that the input from the LCSR has a negligible impact. As expected, the prediction of  $R(D^*)$  using the lattice inputs (combined) has large error and is marginally consistent with the experimental measurement [32]. The error is reduced due to the use of the available inputs on the form factors at  $q^2 = 0$  from LCSR. The inputs from the available experiments considerably reduce the prediction error, and the value is inconsistent with the respective measurements given in eq. 2 or eq. 4.

It is to be noted that the numbers presented in table III are the most up-to-date predictions obtained in the SM. Also, from the results of this table, the predictions can be obtained on the following observables

$$\begin{aligned} \Delta A_{FB}^{D^{(*)}, \ell_i \ell_j} &= A_{FB}^{\bar{B} \rightarrow D^{(*)} \ell_i \nu} - A_{FB}^{\bar{B} \rightarrow D^{(*)} \ell_j \nu} \\ \Delta F_L^{D^*, \ell_i \ell_j} &= F_L^{\bar{B} \rightarrow D^* \ell_i \nu} - F_L^{\bar{B} \rightarrow D^* \ell_j \nu}. \end{aligned} \quad (27)$$

We have predicted these observables in the SM using the results of the fit to lattice (only), which are given below

$$\Delta A_{FB}^{D^*, \mu\tau} = -0.166 \pm 0.010, \quad \Delta A_{FB}^{D^*, \mu e} = 0.004 \pm 0.001, \quad \Delta A_{FB}^{D^*, e\tau} = -0.170 \pm 0.010, \quad (28)$$

$$\Delta A_{FB}^{D, \mu\tau} = -0.3459 \pm 0.0004, \quad \Delta A_{FB}^{D, \mu e} = 0.0137 \pm 0.0001, \quad \Delta A_{FB}^{D, e\tau} = -0.3596 \pm 0.0004, \quad (29)$$



Scenario	$R(D^{(*)})$ from Fall 2022 HFLAV average [31]		$R(D^{(*)})$ from Winter 2023 HFLAV average [32]	
	Fit Parameters	Predictions	Fit Parameters	Predictions
$C_{V_1}$	$C_{V_1}^\tau = 0.08 \pm 0.02$ $C_{V_1}^\mu = \text{unconstrained}$ $ V_{cb}  = (40.3 \pm 0.5) \times 10^{-3}$	$R(D) = 0.349 \pm 0.012,$ $R(D^*) = 0.292 \pm 0.010$ $F_L^{D^*} = 0.453 \pm 0.003$	$C_{V_1}^\tau = 0.07 \pm 0.02$ $C_{V_1}^\mu = \text{unconstrained}$ $ V_{cb}  = (40.3 \pm 0.5) \times 10^{-3}$	$R(D) = 0.344 \pm 0.011,$ $R(D^*) = 0.288 \pm 0.009$ $F_L^{D^*} = 0.453 \pm 0.003$
$C_{V_2}$	$C_{V_2}^\tau = -0.07 \pm 0.03$ $C_{V_2}^\mu = -0.002 \pm 0.014$ $ V_{cb}  = (40.3 \pm 0.6) \times 10^{-3}$	$R(D) = 0.261 \pm 0.017,$ $R(D^*) = 0.283 \pm 0.015$ $F_L^{D^*} = 0.458 \pm 0.003$	$C_{V_2}^\tau = -0.06 \pm 0.03$ $C_{V_2}^\mu = -0.002 \pm 0.014$ $ V_{cb}  = (40.3 \pm 0.6) \times 10^{-3}$	$R(D) = 0.267 \pm 0.016,$ $R(D^*) = 0.279 \pm 0.014$ $F_L^{D^*} = 0.458 \pm 0.003$
$C_T$	$C_T^\tau = -0.05 \pm 0.01$ $C_T^\mu = (0.2 \pm 4.9) \times 10^{-4}$ $ V_{cb}  = (40.3 \pm 0.5) \times 10^{-3}$	$R(D) = 0.288 \pm 0.004,$ $R(D^*) = 0.299 \pm 0.013$ $F_L^{D^*} = 0.439 \pm 0.006$	$C_T^\tau = -0.05 \pm 0.01$ $C_T^\mu = (0.2 \pm 4.9) \times 10^{-4}$ $ V_{cb}  = (40.3 \pm 0.5) \times 10^{-3}$	$R(D) = 0.289 \pm 0.004,$ $R(D^*) = 0.293 \pm 0.012$ $F_L^{D^*} = 0.442 \pm 0.005$
$C_{S_1}$	$C_{S_1}^\tau = 0.152 \pm 0.040$ $C_{S_1}^\mu = -0.004 \pm 0.047$ $ V_{cb}  = (40.3 \pm 0.5) \times 10^{-3}$	$R(D) = 0.388 \pm 0.025,$ $R(D^*) = 0.256 \pm 0.002$ $F_L^{D^*} = 0.463 \pm 0.004$	$C_{S_1}^\tau = 0.153 \pm 0.040$ $C_{S_1}^\mu = -0.004 \pm 0.047$ $ V_{cb}  = (40.3 \pm 0.5) \times 10^{-3}$	$R(D) = 0.388 \pm 0.025,$ $R(D^*) = 0.256 \pm 0.002$ $F_L^{D^*} = 0.463 \pm 0.004$
$C_{S_2}$	$C_{S_2}^\tau = -1.336 \pm 0.044$ $C_{S_2}^\mu = -0.003 \pm 0.046$ $ V_{cb}  = (40.3 \pm 0.5) \times 10^{-3}$	$R(D) = 0.333 \pm 0.024,$ $R(D^*) = 0.307 \pm 0.003$ $F_L^{D^*} = 0.552 \pm 0.005$	$C_{S_2}^\tau = -1.327 \pm 0.044$ $C_{S_2}^\mu = -0.004 \pm 0.046$ $ V_{cb}  = (40.3 \pm 0.5) \times 10^{-3}$	$R(D) = 0.328 \pm 0.024,$ $R(D^*) = 0.306 \pm 0.003$ $F_L^{D^*} = 0.551 \pm 0.005$

TABLE VI: The simultaneous fit of  $|V_{cb}|$  and the new WCs. The inputs are ‘‘Lattice + LCSR( $q^2 = 0$ ) + data on  $\bar{B} \rightarrow D(\mu, e)\bar{\nu}$  and  $\bar{B} \rightarrow D^*(\mu, e)\bar{\nu}$  decays +  $R(D^{(*)}) + F_L^{D^*}$ ’’. These fit assumes different NP in  $\tau$  and  $\mu/e$  final states. Also, we have presented the values of  $R(D^{(*)})$  and  $F_L^{D^*}$  obtained from the fit.

$$\Delta F_L^{D^*, \mu\tau} = 0.053 \pm 0.015, \quad \Delta F_L^{D^*, \mu e} = (0.07 \pm 0.12) \times 10^{-3}, \quad \Delta F_L^{D^*, e\tau} = 0.053 \pm 0.015. \quad (30)$$

Note that  $\Delta A_{FB}^{D^*, \mu e}$  and  $\Delta F_L^{D^*, \mu e}$  are in agreement with the corresponding measured values [16].

In the following we will point out a few other interesting observations from table III:

- For the  $\bar{B} \rightarrow D^*\tau^-\bar{\nu}_\tau$  decays, the predicted values of  $F_L^{\bar{B} \rightarrow D^*\tau^-\bar{\nu}_\tau}$ ,  $A_{\lambda_\tau}^{D^*}$  and  $A_{FB}^{\bar{B} \rightarrow D^*\tau^-\bar{\nu}_\tau}$  in the fit with the experimental data are deviated from those obtained in the fit with only the lattice at  $2.7\sigma$ ,  $1.6\sigma$  and  $2.6\sigma$ , respectively. A similar pattern holds even when we include the LCSR inputs. We need more precise data from the lattice for a robust conclusion.
- Similarly for the  $\bar{B} \rightarrow D^*\mu^-\bar{\nu}$  decays, we can note deviations in the predictions of  $F_L^{\bar{B} \rightarrow D^*\mu^-\bar{\nu}}$ ,  $A_{\lambda_\mu}^{D^*}$  and  $A_{FB}^{\bar{B} \rightarrow D^*\mu^-\bar{\nu}}$  between the fits with or with the experimental data at  $2.3\sigma$ ,  $1.2\sigma$  and  $2.0\sigma$ , respectively. This trend continues for the observables  $F_L^{\bar{B} \rightarrow D^*e^-\bar{\nu}}$  and  $A_{\lambda_e}^{D^*}$ .
- We do not see such deviations in the observables in  $\bar{B} \rightarrow D\mu^-\bar{\nu}$  and  $\bar{B} \rightarrow De^-\bar{\nu}$  decays.
- We have estimated  $\Delta A_{FB}^{D^*, \mu e}$  in the fits with or without the experimental data and noticed that the predictions of  $\Delta A_{FB}^{D^*}$  between these two types of fits differ at  $1.31\sigma$ . In this regard, one could also see the analysis of [5], based on 2018 Belle data. From the results of table III, we have done similar checks for  $\Delta A_{FB}^{D^{(*)}, \mu\tau}$  and  $\Delta A_{FB}^{D^{(*)}, e\tau}$ , also for the  $\Delta F_L^{D^*, \ell_i \ell_j}$ , no significant deviations has been observed.

Following the observations made from the results of table III, we decide to include new physics contributions in the rates of  $\bar{B} \rightarrow D(D^*)\ell^-\bar{\nu}_\ell$  decays for light leptons and repeat the fit with the experimental data mentioned in table III. To understand the impact of the different inputs, we divide our analyses in a couple of scenarios which are the following:

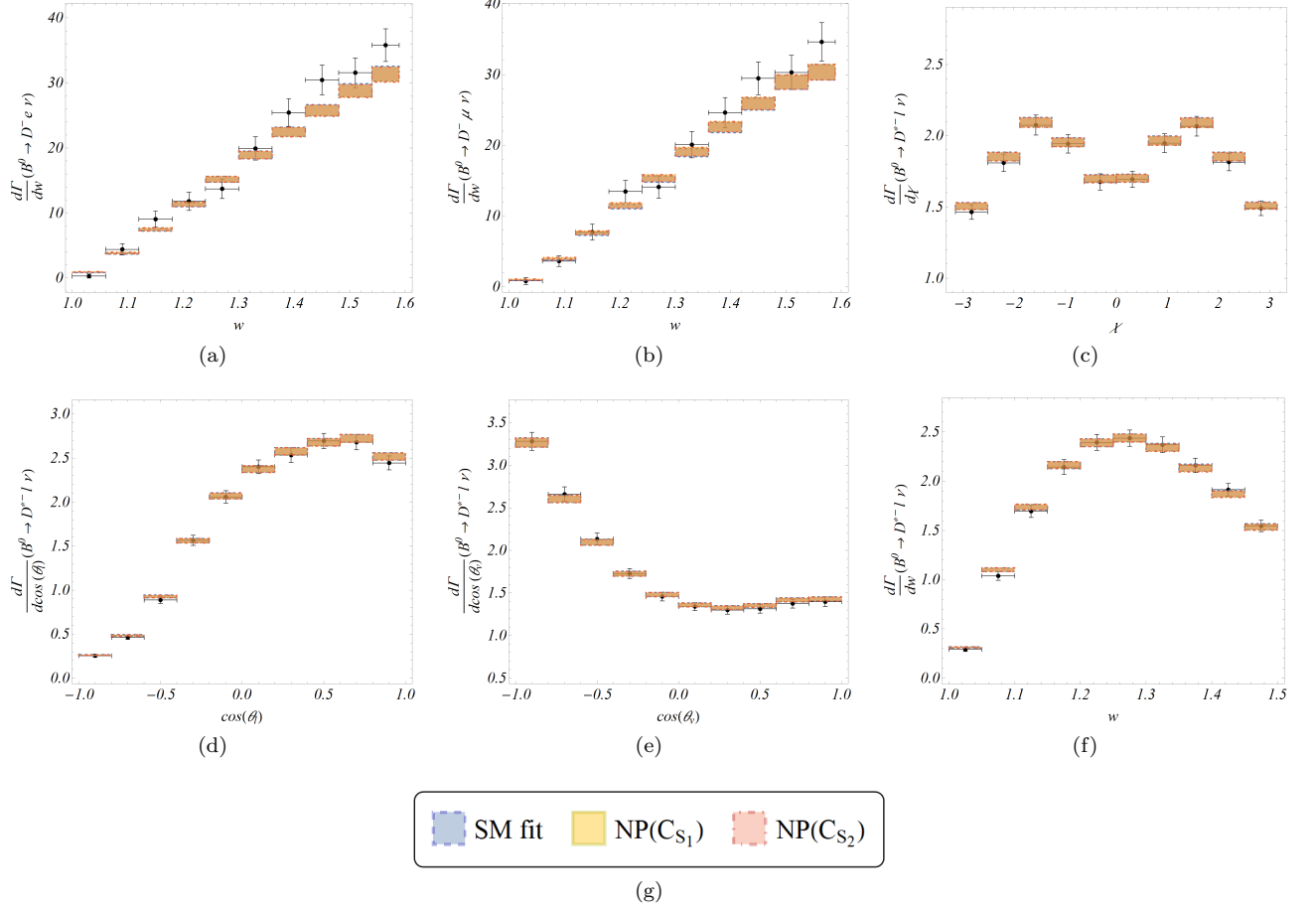


FIG. 1: The predicted angular and  $q^2$  distributions of the rates in  $\bar{B} \rightarrow D(D^*)\ell^-\bar{\nu}_\ell$  decays obtained in the scenarios without NP and with  $C_{S_1}$  and  $C_{S_2}$ , which have been compared with the measured one.

- We have extracted the new WCs directly from a fit to the data in  $\bar{B} \rightarrow D(D^*)\ell^-\bar{\nu}_\ell$ , with  $\ell = \mu$  and  $e$ , alongside the other theory inputs from the lattice and LCSR. The analyses are divided based on whether or not  $R(D^{(*)})$  are included in the fit. For example, the results shown in tables IV are obtained from the fits without the inputs from  $R(D^{(*)})$ . Note that in this fit, we have obtained zero consistent fit values of the new WCs. None of the NP scenarios gives a non-zero NP contribution. The allowed value of  $C_T$  is very small, however, the allowed values of  $C_{V_2}$ ,  $C_{S_1}$  and  $C_{S_2}$  have large errors and the allowed values could be  $\approx 0.05$ . In all the four scenarios, the predicted values of  $R(D)$  and  $R(D^*)$  are consistent with those shown in table III. However, in the scenarios with  $C_{S_1}$  and  $C_{S_2}$ , the predicted value of  $R(D)$  has large errors and the allowed value is  $\lesssim 0.322$  which is close to the lower limit of the measured value at 1- $\sigma$  confidence interval (CI).
- In addition, we have done a couple of other fits including the inputs from  $R(D^{(*)})$  with or without  $F_L^{D^*}$  shown in tables V and VI, respectively.
- For the cases mentioned in the second item, we assume similar or different NP contributions in  $\bar{B} \rightarrow D(D^*)\ell^-\bar{\nu}_\ell$  and  $\bar{B} \rightarrow D^{(*)}\tau^-\bar{\nu}$  decays. The results are shown in table V for similar types of NP. We have not included  $F_L^{D^*}$  in this fit. We have checked that including this input will not change the results. In the other scenario, we have assumed different types of NP contributions in the decays to light and heavy leptons, respectively. In this case, we have presented our results, including  $F_L^{D^*}$  and  $R(D^{(*)})$  in the fits. The corresponding results are shown in table VI. Also, in this case, we have checked that the inclusion of  $F_L^{D^*}$  marginally changes the fit results, and the allowed ranges of the fit parameters are consistent.
- The results in tables IV and V are obtained following two different methods. We have extracted the BGL coefficients alongside the new WCs and  $|V_{cb}|$  in one method. In the other method, the BGL coefficients are obtained from a fit only to the lattice and are kept as nuisance parameters in the fits to the experimental

WC	Fit Parameters	Predictions	WC	Fit Parameters	Predictions
$C_{V_1}$ , $C_{V_2}$	$C_{V_1}^\tau = 0.08 \pm 0.02$ $C_{V_2}^\tau = 0.008 \pm 0.034$ $C_{V_2}^\mu = -0.005 \pm 0.014$ $ V_{cb}  = (40.2 \pm 0.6) \times 10^{-3}$	$R(D) = 0.355 \pm 0.029$ $R(D^*) = 0.284 \pm 0.013$ $F_L^{D^*} = 0.452 \pm 0.004$	$C_{V_2}$ , $C_{S_1}$	$C_{V_2}^\tau = -0.06 \pm 0.03$ $C_{S_1}^\tau = 0.17 \pm 0.04$ $C_{V_2}^\mu = -0.005 \pm 0.014$ $C_{S_1}^\mu = -0.003 \pm 0.048$ $ V_{cb}  = (40.2 \pm 0.6) \times 10^{-3}$	$R(D) = 0.357 \pm 0.029$ $R(D^*) = 0.284 \pm 0.013$ $F_L^{D^*} = 0.468 \pm 0.004$
$C_{V_1}$ , $C_{S_1}$	$C_{V_1}^\tau = 0.06 \pm 0.03$ $C_{S_1}^\tau = 0.04 \pm 0.07$ $C_{S_1}^\mu = -0.003 \pm 0.047$ $ V_{cb}  = (40.3 \pm 0.5) \times 10^{-3}$	$R(D) = 0.358 \pm 0.029$ $R(D^*) = 0.283 \pm 0.013$ $F_L^{D^*} = 0.455 \pm 0.005$	$C_{V_2}$ , $C_{S_2}$	$C_{V_2}^\tau = 0.05 \pm 0.04$ $C_{S_2}^\tau = -1.38 \pm 0.06$ $C_{V_2}^\mu = -0.005 \pm 0.014$ $C_{S_2}^\mu = -0.0005 \pm 0.0474$ $ V_{cb}  = (40.2 \pm 0.6) \times 10^{-3}$	$R(D) = 0.357 \pm 0.029$ $R(D^*) = 0.284 \pm 0.013$ $F_L^{D^*} = 0.557 \pm 0.007$
$C_{V_1}$ , $C_{S_2}$	$C_{V_1}^\tau = -0.05 \pm 0.03$ $C_{S_2}^\tau = -1.37 \pm 0.04$ $C_{S_2}^\mu = -0.002 \pm 0.046$ $ V_{cb}  = (40.3 \pm 0.5) \times 10^{-3}$	$R(D) = 0.357 \pm 0.028$ $R(D^*) = 0.284 \pm 0.013$ $F_L^{D^*} = 0.561 \pm 0.007$	$C_{V_2}$ , $C_T$	$C_{V_2}^\tau = 0.11 \pm 0.05$ $C_T^\tau = -0.09 \pm 0.02$ $C_{V_2}^\mu = -0.003 \pm 0.014$ $C_T^\mu = (0.2 \pm 5.0) \times 10^{-4}$ $ V_{cb}  = (40.3 \pm 0.6) \times 10^{-3}$	$R(D) = 0.348 \pm 0.029$ $R(D^*) = 0.284 \pm 0.013$ $F_L^{D^*} = 0.415 \pm 0.014$
$C_{V_1}$ , $C_T$	$C_{V_1}^\tau = 0.08 \pm 0.03$ $C_T^\tau = 0.01 \pm 0.03$ $C_T^\mu = (0.2 \pm 5.0) \times 10^{-4}$ $ V_{cb}  = (40.3 \pm 0.5) \times 10^{-3}$	$R(D) = 0.357 \pm 0.028$ $R(D^*) = 0.284 \pm 0.013$ $F_L^{D^*} = 0.455 \pm 0.003$	$C_{S_1}$ , $C_T$	$C_{S_1}^\tau = 0.12 \pm 0.05$ $C_T^\tau = -0.03 \pm 0.01$ $C_{S_1}^\mu = -0.003 \pm 0.047$ $C_T^\mu = (0.2 \pm 5.0) \times 10^{-4}$ $ V_{cb}  = (40.3 \pm 0.5) \times 10^{-3}$	$R(D) = 0.359 \pm 0.029$ $R(D^*) = 0.283 \pm 0.013$ $F_L^{D^*} = 0.453 \pm 0.007$
$C_{S_2}$ , $C_{S_1}$	$C_{S_2}^\tau = -0.42 \pm 0.15$ $C_{S_1}^\tau = 0.52 \pm 0.13$ $C_{S_2}^\mu = 0.02 \pm 0.18$ $C_{S_1}^\mu = -0.02 \pm 0.18$ $ V_{cb}  = (40.3 \pm 0.5) \times 10^{-3}$	$R(D) = 0.353 \pm 0.029$ $R(D^*) = 0.287 \pm 0.013$ $F_L^{D^*} = 0.521 \pm 0.021$	$C_{S_2}$ , $C_T$	$C_{S_2}^\tau = -1.36 \pm 0.05$ $C_T^\tau = 0.04 \pm 0.02$ $C_{S_2}^\mu = -0.002 \pm 0.046$ $C_T^\mu = (0.2 \pm 5.0) \times 10^{-4}$ $ V_{cb}  = (40.3 \pm 0.5) \times 10^{-3}$	$R(D) = 0.357 \pm 0.029$ $R(D^*) = 0.284 \pm 0.013$ $F_L^{D^*} = 0.564 \pm 0.008$

TABLE VII: Predictions of  $R(D)$ ,  $R(D^*)$  and  $F_L^{D^*}$  in the two operator scenarios considering different new physics in  $\tau(\mu)$  channels

data. Note that in both methods, the extracted values of the WCs and  $|V_{cb}|$  are the same in the fits with the experimental inputs on  $R(D^{(*)})$  as seen from table V. Also, in the fits without any inputs from  $R(D^{(*)})$ , the results in both methods are not identical but agree. Hence, for the rest of the fits with the inputs on  $R(D^{(*)})$ , we have considered the BGL coefficients as nuisance parameters which will correctly reproduce the respective SM values without any experimental biases.

- As seen from table VI, we have done the analyses using both the HFLAV 2022 and 2023 averages on  $R(D^{(*)})$  and compared the results. As mentioned in the introduction, the 2023 average on  $R(D^*)$  includes the most recent measurement of LHCb, which is yet to be published.
- In all the fits, we have extracted  $|V_{cb}|$  alongside the new WCs. Therefore, it will be difficult to extract simultaneously both  $|V_{cb}|$  and  $C_{V_1}$ , which is clear from the expressions of the decay rate distributions. Also, note that the extracted values of  $|V_{cb}|$  in the fit with  $R(D^{(*)})$  (tables V and VI) are very much consistent with those obtained in the fits without  $R(D^{(*)})$  (table IV). Also, the extracted values of  $|V_{cb}|$  are consistent with the one obtained from the fit without NP.

Obs	$C_{V_1}$	$C_{V_2}$	$C_T$	$C_{S_1}$	$C_{S_2}$	$C_{S_1}, C_{S_2}$
$A_{\lambda_\tau}^{\bar{B} \rightarrow D^* \tau^- \bar{\nu}}$	0.506(3)	0.505(3)	0.47(1)	0.479(8)	0.24(1)	0.32(6)
$A_{FB}^{\bar{B} \rightarrow D^* \tau^- \bar{\nu}}$	-0.053(4)	-0.033(10)	0.01(2)	-0.038(5)	0.052(4)	0.03(2)
$A_{\lambda_\tau}^{\bar{B} \rightarrow D \tau^- \bar{\nu}}$	-0.323(3)	-0.323(3)	-0.349(7)	-0.48(3)	-0.38(5)	-0.43(5)
$A_{FB}^{\bar{B} \rightarrow D \tau^- \bar{\nu}}$	0.3600(2)	0.3599(2)	0.342(5)	0.337(7)	-0.2724(5)	0.346(8)
$A_{\lambda_\mu}^{\bar{B} \rightarrow D^* \mu^- \bar{\nu}}$	0.9852(2)	0.9852(2)	0.9852(2)	0.985(2)	0.985(2)	0.99(1)
$F_L^{\bar{B} \rightarrow D^* \mu^- \bar{\nu}}$	0.531(3)	0.530(3)	0.531(3)	0.531(3)	0.531(3)	0.530(3)
$A_{FB}^{\bar{B} \rightarrow D^* \mu^- \bar{\nu}}$	-0.209(3)	-0.209(3)	-0.209(3)	-0.209(3)	-0.209(3)	-0.210(5)
$A_{\lambda_\mu}^{\bar{B} \rightarrow D \mu^- \bar{\nu}}$	0.9615(2)	0.9615(2)	0.9615(2)	0.96(2)	0.96(1)	0.96(2)
$A_{FB}^{\bar{B} \rightarrow D \mu^- \bar{\nu}}$	0.01380(8)	0.01378(8)	0.01379(9)	0.014(3)	0.014(3)	0.014(3)

TABLE VIII: Predictions of various observables integrated over the whole  $q^2$  bins in the different NP scenarios in the  $\bar{B} \rightarrow D^{(*)} l \bar{\nu}$  channel.

Scenario	Simultaneous fit with	Fit results with
	$ V_{ub} $	$ V_{ub}  = (3.64 \pm 0.07) \times 10^{-3}$ [60]
$C_{V_1}$	N.A.	$C_{V_1}^\mu = -0.01 \pm 0.03$
$C_{V_2}$	N.A.	$C_{V_2}^\mu = -0.01 \pm 0.03$
$C_T$	$C_T^\mu = 0.13 \pm 0.13$ $ V_{ub}  = (3.42 \pm 0.30) \times 10^{-3}$	$C_T^\mu = -0.06 \pm 0.13$
$C_{S_1}$	$C_{S_1}^\mu = (-0.02 \pm 0.16)$ $ V_{ub}  = (3.60 \pm 0.11) \times 10^{-3}$	$C_{S_1}^\mu = -0.02 \pm 0.10$
$C_{S_2}$	$C_{S_2}^\mu = -0.02 \pm 0.16$ $ V_{cb}  = (3.60 \pm 0.11) \times 10^{-3}$	$C_{S_2}^\mu = -0.02 \pm 0.10$

TABLE IX: The extractions of new physics WCs from a fit to the data on rates in  $\bar{B} \rightarrow \pi \ell^- \bar{\nu}_\ell$  decays and the relevant inputs on the respective form factors. In one fit,  $|V_{ub}|$  has been extracted simultaneously with the WCs. In another fit, the value  $|V_{ub}| = (3.64 \pm 0.07) \times 10^{-3}$  from CKMfitter [60] has been used as input.

A few additional observations from the analyses discussed above and the results presented in table V:

- The fits include the inputs from  $R(D^{(*)})$ . The results of table V shows that in the case of identical NP WCs for light and heavy lepton final states, only non-zero solutions are allowed for the four-fermi operators with  $(S \pm P)$  quark current. The fitted values of  $C_{S_1}$  and  $C_{S_2}$  have relatively small errors, and the predicted values of  $R(D)$  can accommodate the respective measured value. However, we do not see the shift in the respective values of  $R(D^{(*)})$  from those presented in table IV. In the other two cases, the solutions are zero consistent, though the data allows large values of  $C_{V_2}$ .
- In the case of  $C_{V_2}$  and  $C_T$ , the predicted values of  $R(D^{(*)})$  are consistent with the SM, and no deviations are observed.
- In the scenarios with scalar and pseudoscalar operators, we have also predicted the angular and the  $q^2$ -distributions of the rates of  $\bar{B} \rightarrow D(D^*) \ell^- \bar{\nu}_\ell$  ( $\ell =$  light leptons) decays in small bins, which are presented in figure 1. The predicted distributions have been compared with the measured values and with the respective predictions obtained from the results of the fits without NP contributions. We do not observe any deviations with respect to SM predictions for the light leptons, which is not surprising since the scalar and pseudoscalar contributions are proportional to the mass of the respective leptons.

Scenario	Simultaneous fit with the CKM elements	Fits with $ V_{ub}  = (3.64 \pm 0.07) \times 10^{-3}$ $ V_{cb}  = (41.1 \pm 0.7) \times 10^{-3}$
	Fit Parameters ( $\frac{\tilde{c}}{\Lambda^2}$ )	Fit Parameters ( $\frac{\tilde{c}}{\Lambda^2}$ )
$C_{V_1}$	$ V_{ub}  = (3.60 \pm 0.11) \times 10^{-3}$ $ V_{cb}  = (40.3 \pm 0.5) \times 10^{-3}$ $\tilde{C}_{\tau q}^{(3)b \rightarrow c} / \Lambda^2 = (-0.48 \pm 0.12) \times 10^{-7}$	$\tilde{C}_{\tau q}^{(3)b \rightarrow c} / \Lambda^2 = (-0.35 \pm 0.15) \times 10^{-7}$ $\tilde{C}_{\mu q}^{(3)b \rightarrow c} / \Lambda^2 = (0.14 \pm 0.09) \times 10^{-7}$ $\tilde{C}_{\mu q}^{(3)b \rightarrow u} / \Lambda^2 = (0.06 \pm 0.20) \times 10^{-8}$
$C_{V_2}$	$ V_{ub}  = (3.60 \pm 0.11) \times 10^{-3}$ $ V_{cb}  = (40.3 \pm 0.6) \times 10^{-3}$ $\tilde{C}_{\phi ud}^{b \rightarrow c} / \Lambda^2 = (-0.06 \pm 0.18) \times 10^{-7}$	$\tilde{C}_{\phi ud}^{b \rightarrow c} / \Lambda^2 = (0.05 \pm 0.17) \times 10^{-7}$ $\tilde{C}_{\phi ud}^{b \rightarrow u} / \Lambda^2 = (-0.01 \pm 0.04) \times 10^{-7}$
$C_{S_1}$	$ V_{ub}  = (3.60 \pm 0.11) \times 10^{-3}$ $ V_{cb}  = (40.3 \pm 0.5) \times 10^{-3}$ $\tilde{C}_{\tau edq}^{*b \rightarrow c} / \Lambda^2 = (-2.02 \pm 0.56) \times 10^{-7}$ $\tilde{C}_{\mu edq}^{*b \rightarrow c} / \Lambda^2 = (0.05 \pm 0.64) \times 10^{-7}$ $\tilde{C}_{\mu edq}^{*b \rightarrow u} / \Lambda^2 = (0.02 \pm 0.21) \times 10^{-7}$	$\tilde{C}_{\tau edq}^{*b \rightarrow c} / \Lambda^2 = (-2.03 \pm 0.57) \times 10^{-7}$ $\tilde{C}_{\mu edq}^{*b \rightarrow c} / \Lambda^2 = (0.08 \pm 0.60) \times 10^{-7}$ $\tilde{C}_{\mu edq}^{*b \rightarrow u} / \Lambda^2 = (0.02 \pm 0.13) \times 10^{-7}$
$C_{S_2}$	$ V_{ub}  = (3.60 \pm 0.11) \times 10^{-3}$ $ V_{cb}  = (40.3 \pm 0.5) \times 10^{-3}$ $\tilde{C}_{\tau equ}^{*(1)b \rightarrow c} / \Lambda^2 = (1.77 \pm 0.06) \times 10^{-6}$ $\tilde{C}_{\mu equ}^{*(1)b \rightarrow c} / \Lambda^2 = (0.06 \pm 0.61) \times 10^{-7}$ $\tilde{C}_{\mu equ}^{*(1)b \rightarrow u} / \Lambda^2 = (0.02 \pm 0.20) \times 10^{-7}$	$\tilde{C}_{\tau equ}^{*(1)b \rightarrow c} / \Lambda^2 = (1.81 \pm 0.06) \times 10^{-6}$ $\tilde{C}_{\mu equ}^{*(1)b \rightarrow c} / \Lambda^2 = (0.09 \pm 0.58) \times 10^{-7}$ $\tilde{C}_{\mu equ}^{*(1)b \rightarrow u} / \Lambda^2 = (0.02 \pm 0.12) \times 10^{-7}$
$C_T$	$ V_{ub}  = (3.44 \pm 0.26) \times 10^{-3}$ $ V_{cb}  = (40.3 \pm 0.5) \times 10^{-3}$ $\tilde{C}_{\tau equ}^{*(3)b \rightarrow c} / \Lambda^2 = (0.61 \pm 0.17) \times 10^{-7}$ $\tilde{C}_{\mu equ}^{*(3)b \rightarrow c} / \Lambda^2 = (-0.28 \pm 6.57) \times 10^{-10}$ $\tilde{C}_{\mu equ}^{*(3)b \rightarrow u} / \Lambda^2 = (-0.14 \pm 0.12) \times 10^{-7}$	$\tilde{C}_{\tau equ}^{*(3)b \rightarrow c} / \Lambda^2 = (0.62 \pm 0.17) \times 10^{-7}$ $\tilde{C}_{\mu equ}^{*(3)b \rightarrow c} / \Lambda^2 = (-0.33 \pm 6.61) \times 10^{-10}$ $\tilde{C}_{\mu equ}^{*(3)b \rightarrow u} / \Lambda^2 = (0.07 \pm 0.16) \times 10^{-7}$

TABLE X: Values of SMEFT coefficients in various scenarios. The fixed values of  $|V_{ub}|$  and  $|V_{cb}|$  are taken from [60].

From the results of table VI, we have the following important observations:

- Table VI presents the fit results considering different new WCs in the heavy and light lepton channels, respectively. In this analysis, we have included the measured value of  $F_L^{D^*}$  alongside other inputs mentioned above. Note that in all the cases, non-zero values of the WCs are allowed in  $\bar{B} \rightarrow D^{(*)}\tau^-\bar{\nu}$  decays. However, for the decays with the light leptons, the allowed values of the WCs are zero consistent. Here,  $C_i^\tau$  represents the WC in the decays with a  $\tau$  in the final state, while  $C_i^\mu$  represents that in the decays with a muon in the final states.
- It is to be noted that only the one operator scenario  $\mathcal{O}_{V_1}$  can explain both the measured values of  $R(D)$  and  $R(D^*)$  simultaneously, but not  $F_L^{D^*}$ . The rest of the one-operator scenarios can only partially explain one observation. For example the one operator scenarios  $\mathcal{O}_{V_2}$  and  $\mathcal{O}_T$  could explain the observation on  $R(D^*)$  but not the  $R(D)$ . None of these scenarios can accommodate the measured value of  $F_L^{D^*}$ . Similarly, the scenario with  $\mathcal{O}_{S_1}$  or  $\mathcal{O}_{S_2}$  can accommodate the observation in  $R(D)$  but not the  $R(D^*)$ . Also, amongst all the one operator scenarios, only  $\mathcal{O}_{S_2}$  can accommodate the measured value of  $F_L^{D^*}$ . In addition, note that the required value of  $C_{S_2}^\tau$  has a magnitude of order one and negative.
- As we have noted, none of the one operator scenarios can accommodate all the three measurements in  $B \rightarrow D^{(*)}$  decays which was the case with the old data as well [47, 61–63]. Hence, an obvious extension will be to look for the two operator scenarios which might accommodate all the three measured values. The results of the fits

with two operator scenarios are shown in table VII. Note that all the two operator scenarios can explain the measured values of both  $R(D)$  and  $R(D^*)$ . However, only the scenarios with  $\mathcal{O}_{S_2}$  as one of the operators could explain  $R(D^*)$  and  $F_L^{D^*}$ . To conclude it further, we have to wait for more precise data on  $D^*$  polarization.

- Note that apart from the scenario  $[\mathcal{O}_{S_1}, \mathcal{O}_{S_2}]$ , in the rest of the two operator scenarios with  $\mathcal{O}_{S_2}$ , we have obtained a branching fraction  $\mathcal{B}(B_c \rightarrow \tau\nu_\tau) \approx 80\%$  which is a relatively high value. Regarding the allowed ranges of  $\mathcal{B}(B_c \rightarrow \tau\nu_\tau)$  the reader could see the refs. [61, 64]. In the scenario  $[\mathcal{O}_{S_1}, \mathcal{O}_{S_2}]$ , the  $\mathcal{B}(B_c \rightarrow \tau\nu_\tau) = 0.50 \pm 0.23$  and the scenarios without  $\mathcal{O}_{S_2}$  have  $\mathcal{B}(B_c \rightarrow \tau\nu_\tau) \lesssim 10\%$ . Hence, if a future measurement does not allow a very large value of this branching fraction, then the only two operator scenario  $[\mathcal{O}_{S_1}, \mathcal{O}_{S_2}]$  will be allowed by all the data.

We have also done a fit where we have considered  $|V_{cb}| = (41.1 \pm 0.7) \times 10^{-3}$  as input which has been taken from the CKMfitter [60]. This  $|V_{cb}|$  value has been obtained from fitting the Wolfenstein parameters from measurements of the modes other than  $b \rightarrow c\ell^-\bar{\nu}_\ell$  semileptonic decays. This fit, in particular, is required to extract the new physics contribution  $C_{V_1}$ , which is otherwise challenging to fit. The constraints obtained on  $C_{V_1}^\tau$  and  $C_{V_1}^\mu$  are given by

$$C_{V_1}^\tau = 0.10 \pm 0.02, \quad C_{V_1}^\mu = 0.03 \pm 0.01. \quad (31)$$

Note that in this scenario, we need non-zero solutions for both the WCs allowed by the available data.

In table VIII, apart from  $R(D^*)$  and  $F_L^{D^*}$ , we have predicted all the  $q^2$  integrated observables listed in table III in the NP scenarios given in table VI. The BGL coefficients and the WCs are obtained from the fit results of table VI. These results should also be compared with the predictions obtained from a fit to data without any NP presented in table III. The future measurements of these observables can be compared with the respective predicted values, the outcome of which for the  $\tau$  final states could be helpful to pinpoint the types of NP interactions. For example, we can see that the forward-backward asymmetry in  $B \rightarrow D^*$  decays has significant deviations only for the scenarios  $C_{V_2}$  or  $C_T$  or  $C_{S_1}$ . On the other hand, for the forward-backward asymmetry in  $B \rightarrow D$ , the deviations will be observed for  $C_{S_1}$  or  $C_{S_2}$  or  $C_T$ . Similarly, in the one operator scenario  $\mathcal{O}_{S_2}$  we observe significant deviations in  $\tau$  polarization in  $B \rightarrow D^*$ . On the other hand, significant deviation in  $\tau$  polarization asymmetry has been observed in the one operator scenario  $\mathcal{O}_{S_1}$  in  $B \rightarrow D$  decays. Also, we have presented the results for the two operator scenario  $[\mathcal{O}_{S_1}, \mathcal{O}_{S_2}]$  and significant deviations are noted for both the  $\tau$  polarization asymmetries and the forward-backward asymmetry in  $B \rightarrow D^*$ . The predictions of these  $q^2$  integrated observables in the other two operator scenarios are presented in the appendix in tables XIII, XIV, XV and XVI, respectively. The pattern of these results could be compared with those given in table III for a test of NP sensitivities. Also, we have predicted the corresponding observables in  $\bar{B} \rightarrow D^*(\mu^-\bar{\nu})$  decays using the fit results given in table VI. The predicted values should be compared with the SM predictions and those obtained in table III without NP. Note that the fitted values of the corresponding WCs do not allow significant deviations of these observables in  $\bar{B} \rightarrow D^*(\mu^-\bar{\nu})$  decays. In the appendix, we have presented the expressions for  $R(D^*)$ ,  $F_L^{D^*}$  and the other related observables in the presence of the NP which could be useful for different phenomenological analysis. In those expressions, we have considered  $C_i^\tau \neq 0$ , however,  $C_i^{\mu,e} = 0$ .

The predictions in small  $q^2$  bins are also obtained which are presented in tables XI, XII for the one operator scenarios. The respective predictions in the two operator scenarios are given in tables XIII, XIV for  $B \rightarrow D$ , and in tables XV and XVI for  $B \rightarrow D^*$  decays, respectively. In all the tables we have presented the corresponding SM predictions which are based on the form factors obtained from the lattice inputs. From the table one can read the  $q^2$ -bin wise NP sensitivities of different observables in  $\bar{B} \rightarrow D^*(\tau^-\bar{\nu})$  decays.

Before we explain the fit of the SMEFT WCs, and the scale  $\Lambda$ , we would like to focus on  $\bar{B} \rightarrow \pi\ell^-\bar{\nu}_\ell$  decays. Like  $\bar{B} \rightarrow D(D^*)\ell^-\bar{\nu}_\ell$  decays, we have extracted  $|V_{ub}|$  alongside the new WCs from the available inputs on  $\bar{B} \rightarrow \pi\ell^-\bar{\nu}_\ell$  decays. Also, we have simultaneously extracted the BSZ coefficients, which we have presented in a separate file. The fit results are shown in table IX. Here, we have followed two different approaches. We have extracted  $|V_{ub}|$  alongside the new WCs and BSZ coefficients in one method. In the other method, we have considered  $|V_{ub}| = (3.64 \pm 0.07) \times 10^{-3}$  [60] as input which has been obtained from the Wolfenstein parameters obtained from a fitting to the available inputs other than the measured value of  $|V_{ub}|$ . In the simultaneous fit, we can not extract  $C_{V_1}^\mu$  and  $C_{V_2}^\mu$ . However, the rest of the WCs can be extracted. Note that in such fits, the extracted values of  $C_{S_1}^\mu$  and  $C_{S_2}^\mu$  are consistent with zero. While the fitted value of  $C_T^\mu$  is marginally consistent with zero, in this case, the extracted value of  $|V_{ub}|$  is lower than the one obtained in the fit without any NP. In all these three cases, large values of WCs are allowed. In the other method, we can extract  $C_{V_1}^\mu$  and  $C_{V_2}^\mu$  on top of the other one operator scenarios. Also, in this method with a fixed  $|V_{ub}|$ , in all the one-operator scenarios, the extracted values of the new WCs are consistent with zero and could be large. The extracted values of  $C_{V_1}^\mu$  and  $C_{V_2}^\mu$  could be smaller than those in  $C_{T,S_1,S_2}^\mu$ . The SM predictions of the associated observables can be seen from the ref. [65]. In this reference, the fit did not include any new physics contribution in  $b \rightarrow u\ell^-\bar{\nu}$  decays. Here, we have predicted the relevant observables in small  $q^2$  bins, which are presented in table XVII in the appendix.

Finally, we have extracted the ratio  $\tilde{C}/\Lambda^2$ , defined in the SMEFT, from the data on  $\bar{B} \rightarrow D(D^*)\ell^-\bar{\nu}_\ell$  and  $\bar{B} \rightarrow \pi\ell^-\bar{\nu}_\ell$  both from theory and experiments. Here,  $\tilde{C}$ s are the couplings of the different dimension-6 operators defined in eq. 9, and  $\Lambda$  is the scale of the new physics. The corresponding WCs at the scale  $m_b$  are defined in eqs. 10 and 11, respectively, for  $b \rightarrow c$  and  $b \rightarrow u$  transitions. We divide this part of the analysis into two broad categories. In one of them, we have fitted the ratio  $\tilde{C}/\Lambda^2$  along with  $|V_{ub}|$  and  $|V_{cb}|$  and in another, for the fixed values of these CKM elements directly. The results are shown in table X. As mentioned earlier, we can not simultaneously extract the CKM elements and  $\tilde{C}_{\mu q}^3$ . However, in the fit for fixed values of the CKM elements, we could simultaneously extract  $\tilde{C}_{\tau q}^3$  and  $\tilde{C}_{\mu q}^3$ , respectively. The general trend shows that the couplings associated with the  $b \rightarrow u$  decays with light leptons are more tightly constrained than similar couplings in  $b \rightarrow c$  decays. Also, within their allowed ranges, apart from  $\tilde{C}_{\mu equ}^{*(3)b \rightarrow u}$  in the rest of the couplings  $\tilde{C}^{b \rightarrow u} < \tilde{C}^{b \rightarrow c}$ , the coupling  $\tilde{C}_{\mu equ}^{*(3)b \rightarrow u} \gg \tilde{C}_{\mu equ}^{*(3)b \rightarrow c}$ . Also, we notice that the couplings associated with the  $\tau$  are one order of magnitude larger than the similar couplings with the  $\mu$ s. However,  $\tilde{C}_{\mu equ}^{*(3)b \rightarrow c} \lesssim 10^{-3} \times \tilde{C}_{\tau equ}^{*(3)b \rightarrow c}$ .

#### IV. RENORMALIZATION-GROUP RUNNING OF THE WILSON COEFFICIENTS

Note that the bounds obtained on the new WCs from data will be relevant at the scale  $m_b$ . Having extracted the Wilson coefficients at the low energy scale ( $\mu \sim m_b$ ), it is very interesting to check their behaviour at high energy scales ( $\mu \gtrsim 1$  TeV) which are accessible at the colliders. For this, it is necessary to solve the renormalization-group (RG) evolution equations of the WCs. The anomalous dimension matrices corresponding to  $\mathcal{O}_{V_1}$  and  $\mathcal{O}_{V_2}$  vanish, thus the corresponding WCs are scale independent and don't mix with the other operators ( $\mathcal{O}_{S_1}, \mathcal{O}_{S_2}$  and  $\mathcal{O}_T$ ) [52, 66]. The RG evolution for the coefficients  $C_i = (C_{S_1}, C_{S_2}$  and  $C_T)$  at the one-loop level from  $\mu_{NP}$  to  $\mu_{MZ}$  is given as [66–69]

$$\frac{dC_i(\mu)}{d \ln \mu} = \frac{1}{16\pi^2} [g_s(\mu)^2 \gamma_s^T + \gamma_w^T(\mu) + y_t(\mu)^2 \gamma_t^T]_{ij} C_j(\mu), \quad (32)$$

with

$$\gamma_s^T = \{\gamma_S, \gamma_S, \gamma_T\}_{\text{diag}}, \quad (33)$$

$$\gamma_w^T(\mu) = \begin{pmatrix} -\frac{8}{3}g^2(\mu) & 0 & 0 \\ 0 & -\frac{11}{3}g^2(\mu) & 18g^2(\mu) + 30g'^2(\mu) \\ 0 & \frac{3}{8}g^2(\mu) + \frac{5}{8}g'^2(\mu) & -3g^2(\mu) + \frac{2}{9}g'^2(\mu) \end{pmatrix}, \quad (34)$$

$$\gamma_t^T = \{0, 1/2, 1/2\}_{\text{diag}}, \quad (35)$$

where  $\gamma_S = -6C_F = -8$  and  $\gamma_T = 2C_F = 8/3$ . Here,  $y_t(\mu)$  refers to the energy scale dependence of the top Yukawa coupling. Its RG running is dominated by QCD corrections, and a subdominant contribution comes from the top Yukawa itself [70]

$$\frac{dy_t}{dt} = \frac{y_t}{16\pi^2} \left( \frac{9}{2}y_t^2 - 8g_s^2 - \frac{9}{4}g^2 - \frac{17}{20}g'^2 \right) \quad (36)$$

with  $t = \ln[\mu]$ . From eq 34, we see that there is operator mixing between  $\mathcal{O}_{S_2}$  and  $\mathcal{O}_T$  which arises from the electroweak anomalous dimension above the electroweak symmetry breaking scale. On the other hand, the main contributions to RG evolution below the electroweak scale come from QCD. In ref. [67] (also see [71]), a numerical solution for the RG evolution is provided at the three-loop in QCD and the one-loop in QED

$$\begin{pmatrix} C_{S_1}(\mu_b) \\ C_{S_2}(\mu_b) \\ C_T(\mu_b) \end{pmatrix} \simeq \begin{pmatrix} 1.46 & 0 & 0 \\ 0 & 1.46 & -0.0177 \\ 0 & -0.0003 & 0.878 \end{pmatrix} \begin{pmatrix} C_{S_1}(m_Z) \\ C_{S_2}(m_Z) \\ C_T(m_Z) \end{pmatrix}. \quad (37)$$

Thus, using the equations 32 and 37, we will get the relation between the WCs at  $\mu_{NP}$  and  $\mu_b$ . In figs. 2a, 2b and 2c, we show the variation of the WCs  $C_{S_1}^T$ ,  $C_{S_2}^T$  and  $C_T^T$  with the energy scale, taking the values of the WCs at  $\mu_b$  from table VI. These projected bounds will be useful in collider searches.

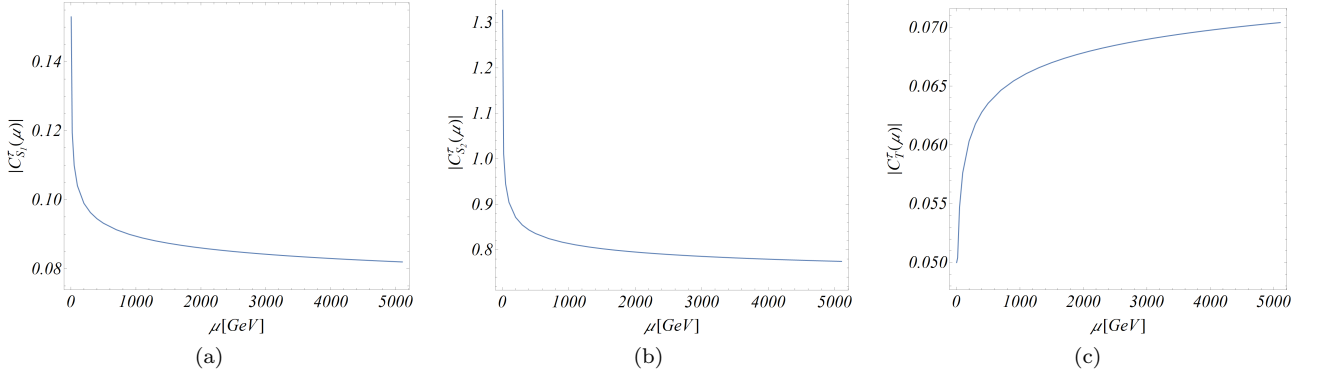


FIG. 2: The variation of the WCs  $C_{S_1}^\tau$ ,  $C_{S_2}^\tau$  and  $C_T^\tau$  with the energy scale  $\mu$ .

## V. SUMMARY

This paper considers NP effects in the  $\bar{B} \rightarrow D(D^*)\ell^-\bar{\nu}_\ell$  decays with the heavy ( $\tau$ ) and light ( $\mu, e$ ) leptons. The analyses include the most up-to-date results from the experiments and the lattice. For example, inputs from the lattice include the  $B \rightarrow D^*$  form factors at non-zero recoils. Also, amongst the data, the most updated results on  $R(D^{(*)})$  and  $d\Gamma(\bar{B} \rightarrow D^*(\mu^-, e^-)\bar{\nu})/dq^2$  are included in the fits. We review the standard model (SM) predictions of the different observables, like  $R(D^{(*)})$ ,  $A_{FB}^{D^{(*)}}$ ,  $P_\ell^{D^{(*)}}$ , and  $F_L^{D^*}$  related to these decay channels with  $\tau$ ,  $\mu$  and  $e$ . Our predictions of the  $R(D^{(*)})$  based on the lattice and LCSR inputs are given as

$$R(D) = 0.304 \pm 0.003, \quad R(D^*) = 0.253 \pm 0.009.$$

Whereas the results obtained using only the lattice inputs are given by

$$R(D) = 0.304 \pm 0.003, \quad R(D^*) = 0.258 \pm 0.012.$$

For all the different lepton final states, we have noticed that the predicted values of  $F_L^{\bar{B} \rightarrow D^*\ell^-\bar{\nu}}$  and  $A_{FB}^{\bar{B} \rightarrow D^*\ell^-\bar{\nu}}$  between the fits with or without the experimental data deviate from each other. For the decays to  $\tau$ , it is  $\gtrsim 2\sigma$  while for the  $\mu$  and  $e$  it is  $\sim 2\sigma$ . Also, we have predicted in the SM the differences  $\Delta A_{FB}^{D^{(*)}}$  and  $\Delta F_L^{D^*}$  between the tauons, muons and electrons in different pairs.

From the available data on  $\bar{B} \rightarrow D^{(*)}(\mu^-, e^-)\bar{\nu}$  decays and the available lattice inputs we have simultaneously extracted  $|V_{cb}|$ , the new WCs and the form factors. In all the different NP scenarios, the extracted values of  $|V_{cb}|$  is given by

$$|V_{cb}| = (40.3 \pm 0.5) \times 10^{-3},$$

which is consistent with the fit without NP. In this case, the fitted values of the new WCs are consistent with zero but could be considerable. Only in the scenarios with the WC  $C_{S_1}^\mu$  or  $C_{S_2}^\mu$ , we have noted an enhancement in the predictions of  $R(D)$  (but not in  $R(D^*)$ ) from that of SM but not large enough to explain the  $1\text{-}\sigma$  lower limit of the corresponding data.

Also, we have analysed the most up-to-date data on  $R(D^{(*)})$  with or without  $F_L^{D^*}$  alongside the inputs on  $\Gamma(\bar{B} \rightarrow D^{(*)}(\mu^-, e^-)\bar{\nu})$  decays. In this study, we divide our analyses based on whether there are similar types or different types of NP in the decays with  $\tau$  and  $\mu$  or  $e$  in the final state. In both types of fits, the extracted values of  $|V_{cb}|$  do not shift from the one mentioned above. For similar types of NP, only the one operator scenarios  $\mathcal{O}_{S_1}$  or  $\mathcal{O}_{S_2}$  could explain the observed data in  $R(D)$  but not  $R(D^*)$ . Also, amongst these two scenarios, only the contribution from  $\mathcal{O}_{S_2}$  shows an enhancement in the value of  $F_L^{D^*}$  but not sufficient to explain the respective measured value.

In the case of different types of NP in the heavy and light leptons, the one operator scenario  $\mathcal{O}_{V_1}^\tau$  can accommodate the observations in  $R(D^{(*)})$ . However, it can not explain  $F_L^{D^*}$ . On the other hand, the scenario  $\mathcal{O}_{S_2}^\tau$  can explain  $R(D)$  and  $F_L^{D^*}$  but not  $R(D^*)$ . The scenarios  $\mathcal{O}_{V_{2,T}}^\tau$  can explain only  $R(D^*)$  and the  $\mathcal{O}_{S_1}^\tau$  can explain only  $R(D)$ , not the other two observations. However, all the two operator scenarios with  $\mathcal{O}_{S_2}^\tau$  as one of the operators could explain all the measured values. Note that apart from the scenario  $[\mathcal{O}_{S_1}^\tau, \mathcal{O}_{S_2}^\tau]$ , in all the other two operator scenarios with one of the operator  $\mathcal{O}_{S_2}^\tau$ , the branching fractions  $\mathcal{B}(B_c \rightarrow \tau\nu) \approx 80\%$ . However, in the scenario  $[\mathcal{O}_{S_1}^\tau, \mathcal{O}_{S_2}^\tau]$  the fit result



predicts  $\mathcal{B}(B_c \rightarrow \tau\nu) = 0.50 \pm 0.23$ . The bounds obtained on the new WCs will be relevant at the scale  $m_b$ ; following an RGE, we have projected those bounds to high-scale NP, which could be useful for collider searches.

In addition to  $\bar{B} \rightarrow D(D^*)\ell^-\bar{\nu}_\ell$  decays, we have also studied the available data on  $\bar{B} \rightarrow \pi\ell^-\bar{\nu}_\ell$  decays in the presence of NP. The CKM element  $|V_{ub}|$  has been extracted alongside the new WCs. We have noticed that the extracted new WCs have large errors and are consistent with zero, but large values are allowed by the data. Finally, in the SM and the NP scenarios, we have predicted various observables associated with the above decay modes for the light leptons.

Using all these available data for the light and heavy leptons in  $\bar{B} \rightarrow D(D^*)\ell^-\bar{\nu}_\ell$  and  $\bar{B} \rightarrow \pi\ell^-\bar{\nu}_\ell$  decays, we have given bounds on the couplings of the relevant SMEFT operators and the probable NP scale  $\Lambda$ . We have noticed that in the  $\tau$  channel for the order one magnitude of the couplings ( $\tilde{C}^\tau$ ), the NP scale  $\Lambda \approx 1$  TeV, while for muon channel for a coupling strength  $\tilde{C}^\mu \approx 1$ , we need  $\Lambda \approx 5$  TeV. Therefore, based on the current data, for a fixed value of  $\Lambda$ ,  $\tilde{C}^\tau \approx 10 \times \tilde{C}^\mu$  which is as per the expectation.

## ACKNOWLEDGMENTS

We would like to thank Markus Prim, Florian Bernlochner and Syuhei Iguro for some useful communications.

## VI. APPENDIX

The expressions of  $R(D)$ ,  $R(D^*)$ ,  $F_L^{D^*}$ ,  $A_{FB}^{D^*}$ ,  $A_{\lambda\tau}^{D^*}$ ,  $A_{FB}^D$  and  $A_{\lambda\tau}^D$  in the presence of NP are given in the equations 38, 39, 40, 41, 42, 43 and 44 respectively.

$$\begin{aligned}
R(D) = & (0.304 \pm 0.003) \times (1 + 1.35C_{S_1}^{\tau^2} + C_{S_1}(2.70C_{S_2}^\tau + 1.72C_{V_1}^\tau + 1.72C_{V_2}^\tau + 1.72) + 1.35C_{S_2}^{\tau^2} + \\
& 0.83C_T^\tau C_{V_1}^\tau + C_{S_2}^\tau(1.72C_{V_1}^\tau + 1.72C_{V_2}^\tau + 1.72) + 0.83C_T^\tau C_{V_2}^\tau + (0.49C_T^\tau + 0.83)C_T^\tau + C_{V_1}^{\tau^2} + \\
& 2.00C_{V_1}^\tau C_{V_2}^\tau + 2.00C_{V_1}^\tau + C_{V_2}^{\tau^2} + 2.00C_{V_2}^\tau). \tag{38}
\end{aligned}$$

$$\begin{aligned}
R(D^*) = & (0.258 \pm 0.012) \times (1 + 0.04C_{S_1}^{\tau^2} + C_{S_1}^\tau(-0.07C_{S_2}^\tau + 0.10C_{V_1}^\tau - 0.10C_{V_2}^\tau + 0.10) + 0.04C_{S_2}^{\tau^2} + \\
& C_{S_2}^\tau(-0.10C_{V_1}^\tau + 0.10C_{V_2}^\tau - 0.10) - 2.94C_T^\tau C_{V_1}^\tau + 4.79C_T^\tau C_{V_2}^\tau + C_T^\tau(10.65C_T^\tau - 2.94) + C_{V_1}^{\tau^2} - \\
& 1.79C_{V_1}^\tau C_{V_2}^\tau + 2.C_{V_1}^\tau + C_{V_2}^{\tau^2} - 1.79C_{V_2}^\tau). \tag{39}
\end{aligned}$$

$$\begin{aligned}
F_L^{D^*} = & (0.427 \pm 0.009) \times (27.26 + 2.34C_{S_1}^{\tau^2} + C_{S_1}^\tau(-4.68C_{S_2}^\tau + 6.65C_{V_1}^\tau - 6.65C_{V_2}^\tau + 6.65) + 2.34C_{S_2}^{\tau^2} - 66.82C_T^\tau C_{V_1}^\tau + \\
& C_{S_2}^\tau(-6.65C_{V_1}^\tau + 6.65C_{V_2}^\tau - 6.65) + 66.82C_T^\tau C_{V_2}^\tau + C_T^\tau(69.62C_T^\tau - 66.82) + 27.26C_{V_1}^{\tau^2} - 54.52C_{V_1}^\tau C_{V_2}^\tau + \\
& 54.52C_{V_1}^\tau + 27.26C_{V_2}^{\tau^2} - 54.52C_{V_2}^\tau)/(27.26 + C_{S_1}^{\tau^2} + C_{S_1}^\tau(-2.C_{S_2}^\tau + 2.84C_{V_1}^\tau - 2.84C_{V_2}^\tau + 2.84) + C_{S_2}^{\tau^2} + \\
& C_{S_2}^\tau(-2.84C_{V_1}^\tau + 2.84C_{V_2}^\tau - 2.84) - 80.15C_T^\tau C_{V_1}^\tau + 130.72C_T^\tau C_{V_2}^\tau + C_T^\tau(290.34C_T^\tau - 80.15) + 27.26C_{V_1}^{\tau^2} - \\
& 48.81C_{V_1}^\tau C_{V_2}^\tau + 54.52C_{V_1}^\tau + 27.26C_{V_2}^{\tau^2} - 48.81C_{V_2}^\tau). \tag{40}
\end{aligned}$$

$$\begin{aligned}
A_{FB}^{D^*} = & (-0.077 \pm 0.009) \times (0.09 + C_{S_1}^\tau(0.27C_T^\tau - 0.10C_{V_1}^\tau + 0.10C_{V_2}^\tau - 0.10) + 0.29C_{V_1}^\tau C_{V_2}^\tau + 0.19C_{V_1}^\tau + 0.26C_{V_2}^\tau + \\
& C_{S_2}^\tau(-0.27C_T^\tau + 0.10C_{V_1}^\tau - 0.10C_{V_2}^\tau + 0.10) - 4.19C_T^{\tau^2} + 1.50C_T^\tau C_{V_1}^\tau - 2.63C_T^\tau C_{V_2}^\tau + 1.50C_T^\tau + 0.09C_{V_1}^{\tau^2} + \\
& - 0.38C_{V_2}^{\tau^2})/(0.09 + 0.003C_{S_1}^{\tau^2} + C_{S_1}^\tau(-0.01C_{S_2}^\tau + 0.01C_{V_1}^\tau - 0.01C_{V_2}^\tau + 0.01) + 0.003C_{S_2}^{\tau^2} + 0.19C_{V_1}^\tau + \\
& C_{S_2}^\tau(-0.01C_{V_1}^\tau + 0.01C_{V_2}^\tau - 0.01) - 0.28C_T^\tau C_{V_1}^\tau + 0.45C_T^\tau C_{V_2}^\tau + C_T^\tau(C_T^\tau - 0.28) + 0.09C_{V_1}^{\tau^2} - 0.17C_{V_1}^\tau C_{V_2}^\tau + \\
& 0.09C_{V_2}^{\tau^2} - 0.17C_{V_2}^\tau) \tag{41}
\end{aligned}$$

$$\begin{aligned}
A_{\lambda_\tau}^{D^*} = & (0.519 \pm 0.007) \times (3.29 - 0.23C_{S_1}^{\tau^2} + C_{S_1}^\tau(0.46C_{S_2}^\tau - 0.66C_{V_1}^\tau + 0.66C_{V_2}^\tau - 0.66) - 0.23C_{S_2}^{\tau^2} + 3.29C_{V_2}^{\tau^2} + \\
& C_{S_2}^\tau(0.66C_{V_1}^\tau - 0.66C_{V_2}^\tau + 0.66) - 6.21C_T^\tau C_{V_1}^\tau + 10.13C_T^\tau C_{V_2}^\tau + (-3.52C_T^\tau - 6.21)C_T^\tau + 3.29C_{V_1}^{\tau^2} - 5.75C_{V_1}^\tau C_{V_2}^\tau + \\
& 6.58C_{V_1}^\tau - 5.75C_{V_2}^\tau)/(3.29 + 0.12C_{S_1}^{\tau^2} + C_{S_1}^\tau(-0.24C_{S_2}^\tau + 0.34C_{V_1}^\tau - 0.34C_{V_2}^\tau + 0.34) + 0.12C_{S_2}^{\tau^2} + 6.58C_{V_1}^\tau \\
& C_{S_2}^\tau(-0.34C_{V_1}^\tau + 0.34C_{V_2}^\tau - 0.34) - 9.67C_T^\tau C_{V_1}^\tau + 15.77C_T^\tau C_{V_2}^\tau + C_T^\tau(35.02C_T^\tau - 9.67) + 3.29C_{V_1}^{\tau^2} - 5.89C_{V_1}^\tau C_{V_2}^\tau + \\
& 3.29C_{V_2}^{\tau^2} - 5.89C_{V_2}^\tau)
\end{aligned} \tag{42}$$

$$\begin{aligned}
A_{FB}^D = & (0.3596 \pm 0.0004) \times (2.06 + C_{S_1}^\tau(5.61C_T^\tau + 2.84C_{V_1}^\tau + 2.84C_{V_2}^\tau + 2.84) + 3.82C_T^\tau C_{V_1}^\tau + 3.82C_T^\tau C_{V_2}^\tau + 3.82C_T^\tau + \\
& C_{S_2}^\tau(5.61C_T^\tau + 2.84C_{V_1}^\tau + 2.84C_{V_2}^\tau + 2.84) + 2.06C_{V_1}^{\tau^2} + 4.12C_{V_1}^\tau C_{V_2}^\tau + 4.12C_{V_2}^\tau + 2.06C_{V_2}^{\tau^2} + 4.12C_{V_2}^\tau)/(2.06 + \\
& 2.78C_{S_1}^{\tau^2} + C_{S_1}^\tau(5.57C_{S_2}^\tau + 3.54C_{V_1}^\tau + 3.54C_{V_2}^\tau + 3.54) + 2.78C_{S_2}^{\tau^2} + C_{S_2}^\tau(3.54C_{V_1}^\tau + 3.54C_{V_2}^\tau + 3.54) + 1.71C_T^\tau C_{V_1}^\tau + \\
& 1.71C_T^\tau C_{V_2}^\tau + C_T^\tau(C_T^\tau + 1.71) + 2.06C_{V_1}^{\tau^2} + 4.12C_{V_1}^\tau C_{V_2}^\tau + 4.12C_{V_2}^\tau + 2.06C_{V_2}^{\tau^2} + 4.12C_{V_2}^\tau)
\end{aligned} \tag{43}$$

$$\begin{aligned}
A_{\lambda_\tau}^D = & (-0.324 \pm 0.003) \times (0.74 + 3.09C_{S_1}^{\tau^2} + C_{S_1}^\tau(6.17C_{S_2}^\tau + 3.93C_{V_1}^\tau + 3.93C_{V_2}^\tau + 3.93) + 3.09C_{S_2}^{\tau^2} - 0.63C_T^\tau C_{V_1}^\tau + \\
& C_{S_2}^\tau(3.93C_{V_1}^\tau + 3.93C_{V_2}^\tau + 3.93) - 0.63C_T^\tau C_{V_2}^\tau + (0.07C_T^\tau - 0.63)C_T^\tau + 0.74C_{V_1}^{\tau^2} + 1.48C_{V_1}^\tau C_{V_2}^\tau + 1.48C_{V_1}^\tau + \\
& 0.74C_{V_2}^{\tau^2} + 1.48C_{V_2}^\tau)/(0.74 - 0.63C_T^\tau C_{S_1}^{\tau^2} - 0.63C_T^\tau C_{S_1}^\tau(2.C_{S_2}^\tau + 1.27C_{V_1}^\tau + 1.27C_{V_2}^\tau + 1.27) + C_{S_2}^{\tau^2} + \\
& C_{S_2}^\tau(1.27C_{V_1}^\tau + 1.27C_{V_2}^\tau + 1.27) + 0.61C_T^\tau C_{V_1}^\tau + 0.61C_T^\tau C_{V_2}^\tau + (0.36C_T^\tau + 0.61)C_T^\tau + 0.74C_{V_1}^{\tau^2} + 1.48C_{V_1}^\tau C_{V_2}^\tau + \\
& 1.48C_{V_1}^\tau + 0.74C_{V_2}^{\tau^2} + 1.48C_{V_2}^\tau)
\end{aligned} \tag{44}$$

One can obtain the SM predictions by setting the new WCs  $C_i = 0$ . We have obtained the results for the SM following the fit results of the form factors obtained from only the use of lattice. We have also provided the corresponding errors. We have not quoted the errors associated with the terms of the new WCs. Depending on different models, these expressions are useful in phenomenological analyses to constrain the new physics contributions in the  $C_i$ s. The numerical factors in front of each of the coefficients also depend on the fitted values of the BGL coefficients.

The predictions of the different observables related to  $\bar{B} \rightarrow D^{(*)}(\tau^-, \mu^-, e^-)\bar{\nu}$  and  $\bar{B} \rightarrow \pi\mu^-\bar{\nu}$  decays in the SM and different NP scenarios in small  $q^2$ -bins are presented in this section. In the one operator scenarios, the predictions are presented in tables XI and XII for  $B \rightarrow D$  and  $B \rightarrow D^*$  decays, respectively. The respective predictions in the two operator scenarios are given in tables XIII, XIV for  $B \rightarrow D$ , and in tables XV and XVI for  $B \rightarrow D^*$  decays, respectively. These predictions are obtained using the fit results of tables VI and VII.

- 
- [1] P. Gambino, M. Jung, and S. Schacht, The  $V_{cb}$  puzzle: An update, Phys. Lett. B **795**, 386 (2019), arXiv:1905.08209 [hep-ph].
  - [2] S. Jaiswal, S. Nandi, and S. K. Patra, Updates on extraction of  $-V_{cb}$  and SM prediction of  $R(D^*)$  in  $B \rightarrow D^* \ell \nu_\ell$  decays, JHEP **06**, 165, arXiv:2002.05726 [hep-ph].
  - [3] D. Leljak, D. van Dyk, and B. Melić, The  $\bar{B} \rightarrow \pi$  form factors from QCD and their impact on  $|V_{ub}|$ , (2021), arXiv:2102.07233 [hep-ph].
  - [4] A. Biswas, S. Nandi, S. K. Patra, and I. Ray, A closer look at the extraction of  $-V_{ub}$  from  $B \rightarrow \pi \ell \nu$ , JHEP **07**, 082, arXiv:2103.01809 [hep-ph].
  - [5] C. Bobeth, M. Bordone, N. Gubernari, M. Jung, and D. van Dyk, Lepton-flavour non-universality of  $\bar{B} \rightarrow D^* \ell \bar{\nu}$  angular distributions in and beyond the Standard Model, Eur. Phys. J. C **81**, 984 (2021), arXiv:2104.02094 [hep-ph].
  - [6] G. Martinelli, S. Simula, and L. Vittorio, Exclusive determinations of  $|V_{cb}|$  and  $R(D^*)$  through unitarity, Eur. Phys. J. C **82**, 1083 (2022), arXiv:2109.15248 [hep-ph].
  - [7] G. Martinelli, S. Simula, and L. Vittorio,  $|V_{cb}|$  and  $R(D)^{(*)}$  using lattice QCD and unitarity, Phys. Rev. D **105**, 034503 (2022), arXiv:2105.08674 [hep-ph].
  - [8] F. U. Bernlochner, M. F. Sevilla, D. J. Robinson, and G. Wormser, Semitauconic b-hadron decays: A lepton flavor universality laboratory, Rev. Mod. Phys. **94**, 015003 (2022), arXiv:2101.08326 [hep-ex].
  - [9] G. Martinelli, S. Simula, and L. Vittorio, Exclusive semileptonic  $B \rightarrow \pi \ell \nu_\ell$  and  $B_s \rightarrow K \ell \nu_\ell$  decays through unitarity and lattice QCD, JHEP **08**, 022, arXiv:2202.10285 [hep-ph].

Obs	$q^2$ bins	SM value	$C_{V_1}$	$C_{V_2}$	$C_T$	$C_{S_1}$	$C_{S_2}$
$A_{FB}^{\bar{B} \rightarrow D\mu^- \bar{\nu}}$	{0.01, 2}	0.03319(6)	0.03325(5)	0.03324(5)	0.03324(6)	0.033(2)	0.033(2)
	{2, 4}	0.00649(1)	0.00649(1)	0.00649(1)	0.00649(4)	0.006(3)	0.006(3)
	{4, 6}	0.00423(1)	0.00423(1)	0.00423(1)	0.00423(5)	0.004(3)	0.004(3)
	{6, 8}	0.00350(1)	0.00350(1)	0.00350(1)	0.00350(5)	0.003(4)	0.003(4)
	{8, 10}	0.00348(1)	0.00348(1)	0.00348(1)	0.00348(6)	0.003(5)	0.003(5)
	{10, 11.628}	0.00458(2)	0.00458(2)	0.00459(2)	0.0046(1)	0.004(7)	0.004(7)
$A_{\lambda_\ell}^{\bar{B} \rightarrow D\mu^- \bar{\nu}}$	{0.01, 2}	0.9107(2)	0.9106(1)	0.9106(1)	0.9106(1)	0.911(10)	0.911(10)
	{2, 4}	0.98165(5)	0.98165(5)	0.98165(5)	0.98165(6)	0.98(1)	0.98(1)
	{4, 6}	0.98721(6)	0.98722(5)	0.98722(6)	0.98721(6)	0.99(1)	0.99(1)
	{6, 8}	0.98825(6)	0.98826(6)	0.98826(6)	0.98826(8)	0.99(2)	0.99(2)
	{8, 10}	0.98580(10)	0.98581(9)	0.98580(9)	0.9858(1)	0.99(3)	0.99(3)
	{10, 11.628}	0.9706(2)	0.9706(2)	0.9706(2)	0.9706(2)	0.98(8)	0.98(8)
$A_{FB}^{\bar{B} \rightarrow D\tau^- \bar{\nu}}$	{3.157, 5}	0.44311(8)	0.44315(8)	0.44314(8)	0.436(2)	0.436(3)	-0.13(3)
	{5, 7}	0.39400(8)	0.39404(6)	0.39403(8)	0.381(4)	0.385(3)	-0.33(2)
	{7, 9}	0.3494(2)	0.3494(2)	0.3494(2)	0.329(6)	0.332(6)	-0.339(4)
	{9, 11.628}	0.2848(5)	0.2849(5)	0.2848(5)	0.258(7)	0.248(9)	-0.210(8)
$A_{\lambda_\ell}^{\bar{B} \rightarrow D\tau^- \bar{\nu}}$	{3.157, 5}	-0.314(2)	-0.314(2)	-0.314(2)	-0.340(7)	-0.40(2)	0.43(2)
	{5, 7}	-0.255(2)	-0.255(2)	-0.255(2)	-0.280(7)	-0.38(3)	0.16(6)
	{7, 9}	-0.278(3)	-0.277(3)	-0.277(3)	-0.303(8)	-0.44(4)	-0.32(5)
	{9, 11.628}	-0.496(3)	-0.496(3)	-0.496(3)	-0.520(7)	-0.66(3)	-0.76(2)

TABLE XI: Predictions of various observables in the SM and different 1-operator scenarios in the  $\bar{B} \rightarrow D\ell\bar{\nu}$  channel.

- [10] F. U. Bernlochner, M. T. Prim, and D. J. Robinson,  $B \rightarrow \rho\ell\nu^-$  and  $\omega\ell\nu^-$  in and beyond the Standard Model: Improved predictions and  $-\text{Vub}$ , Phys. Rev. D **104**, 034032 (2021), arXiv:2104.05739 [hep-ph].
- [11] S. González-Solís, P. Masjuan, and C. Rojas, Padé approximants to  $B \rightarrow \pi\ell\nu_\ell$  and  $B_s \rightarrow K\ell\nu_\ell$  and determination of  $|V_{ub}|$ , Phys. Rev. D **104**, 114041 (2021), arXiv:2110.06153 [hep-ph].
- [12] A. Biswas, S. Nandi, and I. Ray, Extractions of  $|V_{ub}|/|V_{cb}|$  from a combined study of the exclusive  $b \rightarrow u(c)\ell\nu_\ell$  decays, (2022), arXiv:2212.02528 [hep-ph].
- [13] R. Glattauer *et al.* (Belle), Measurement of the decay  $B \rightarrow D\ell\nu_\ell$  in fully reconstructed events and determination of the Cabibbo-Kobayashi-Maskawa matrix element  $|V_{cb}|$ , Phys. Rev. D **93**, 032006 (2016), arXiv:1510.03657 [hep-ex].
- [14] A. Abdesselam *et al.* (Belle), Precise determination of the CKM matrix element  $|V_{cb}|$  with  $\bar{B}^0 \rightarrow D^{*+}\ell^- \bar{\nu}_\ell$  decays with hadronic tagging at Belle, (2017), arXiv:1702.01521 [hep-ex].
- [15] E. Waheed *et al.* (Belle), Measurement of the CKM matrix element  $|V_{cb}|$  from  $B^0 \rightarrow D^{*-}\ell^+ \nu_\ell$  at Belle, Phys. Rev. D **100**, 052007 (2019), [Erratum: Phys.Rev.D 103, 079901 (2021)], arXiv:1809.03290 [hep-ex].
- [16] M. T. Prim *et al.* (Belle), Measurement of Differential Distributions of  $B \rightarrow D^*\ell\bar{\nu}_\ell$  and Implications on  $|V_{cb}|$ , (2023), arXiv:2301.07529 [hep-ex].
- [17] P. del Amo Sanchez *et al.* (BaBar), Study of  $B \rightarrow \pi\ell\nu$  and  $B \rightarrow \rho\ell\nu$  Decays and Determination of  $|V_{ub}|$ , Phys. Rev. D **83**, 032007 (2011), arXiv:1005.3288 [hep-ex].
- [18] H. Ha *et al.* (Belle), Measurement of the decay  $B^0 \rightarrow \pi^-\ell^+\nu$  and determination of  $|V_{ub}|$ , Phys. Rev. D **83**, 071101 (2011), arXiv:1012.0090 [hep-ex].
- [19] J. P. Lees *et al.* (BaBar), Branching fraction measurement of  $B^+ \rightarrow \omega\ell^+\nu$  decays, Phys. Rev. D **87**, 032004 (2013), [Erratum: Phys.Rev.D 87, 099904 (2013)], arXiv:1205.6245 [hep-ex].
- [20] J. P. Lees *et al.* (BaBar), Measurement of the  $B^+ \rightarrow \omega\ell^+\nu$  branching fraction with semileptonically tagged B mesons, Phys. Rev. D **88**, 072006 (2013), arXiv:1308.2589 [hep-ex].
- [21] J. Lees *et al.* (BaBar), Branching fraction and form-factor shape measurements of exclusive charmless semileptonic B decays, and determination of  $|V_{ub}|$ , Phys. Rev. D **86**, 092004 (2012), arXiv:1208.1253 [hep-ex].

Obs	$q^2$ bins	SM value	$C_{V_1}$	$C_{V_2}$	$C_T$	$C_{S_1}$	$C_{S_2}$
$A_{FB}^{\bar{B} \rightarrow D^* \mu^- \bar{\nu}}$	{0.01, 2}	-0.08(1)	-0.059(5)	-0.059(5)	-0.059(5)	-0.059(5)	-0.059(5)
	{2, 4}	-0.23(1)	-0.198(5)	-0.198(5)	-0.198(5)	-0.198(5)	-0.198(5)
	{4, 6}	-0.29(1)	-0.259(4)	-0.259(4)	-0.259(4)	-0.259(4)	-0.259(4)
	{6, 8}	-0.290(9)	-0.271(5)	-0.271(5)	-0.271(5)	-0.271(5)	-0.271(5)
	{8, 10}	-0.235(7)	-0.224(5)	-0.223(5)	-0.224(5)	-0.224(5)	-0.224(5)
	{10, 10.68}	-0.128(4)	-0.124(3)	-0.123(3)	-0.124(3)	-0.124(3)	-0.124(3)
$A_{\lambda_\ell}^{\bar{B} \rightarrow D^* \mu^- \bar{\nu}}$	{0.01, 2}	0.930(2)	0.9276(5)	0.9276(5)	0.9276(9)	0.928(4)	0.927(4)
	{2, 4}	0.9905(2)	0.9902(1)	0.9902(1)	0.9902(2)	0.990(3)	0.990(3)
	{4, 6}	0.99564(6)	0.99552(5)	0.99551(5)	0.9955(1)	0.996(2)	0.995(2)
	{6, 8}	0.99750(3)	0.99746(2)	0.99746(2)	0.99746(8)	0.9975(10)	0.997(1)
	{8, 10}	0.99842(1)	0.998410(10)	0.998409(10)	0.99841(8)	0.9984(5)	0.9984(5)
	{10, 10.68}	0.998844(2)	0.998843(2)	0.998843(2)	0.99885(8)	0.9989(1)	0.9988(1)
$F_L^{\bar{B} \rightarrow D^* \mu^- \bar{\nu}}$	{0.01, 2}	0.82(1)	0.848(5)	0.848(5)	0.848(5)	0.848(5)	0.848(5)
	{2, 4}	0.60(2)	0.636(5)	0.636(5)	0.636(5)	0.636(5)	0.636(5)
	{4, 6}	0.47(1)	0.501(3)	0.501(3)	0.501(3)	0.501(3)	0.501(3)
	{6, 8}	0.399(6)	0.415(3)	0.415(3)	0.415(3)	0.415(3)	0.415(3)
	{8, 10}	0.355(3)	0.363(2)	0.363(2)	0.363(2)	0.363(2)	0.362(2)
	{10, 10.68}	0.3371(8)	0.3388(5)	0.3388(5)	0.3388(5)	0.3388(5)	0.3388(5)
$A_{FB}^{\bar{B} \rightarrow D^* \tau^- \bar{\nu}}$	{3.157, 5}	0.09(1)	0.126(4)	0.144(9)	0.17(1)	0.141(5)	0.213(3)
	{5, 7}	-0.034(10)	-0.009(4)	0.01(1)	0.05(2)	0.008(6)	0.105(4)
	{7, 9}	-0.110(7)	-0.095(4)	-0.07(1)	-0.02(2)	-0.080(6)	0.016(5)
	{9, 10.68}	-0.103(5)	-0.095(3)	-0.079(8)	-0.03(2)	-0.087(4)	-0.025(4)
$A_{\lambda_\ell}^{\bar{B} \rightarrow D^* \tau^- \bar{\nu}}$	{3.157, 5}	0.159(8)	0.144(6)	0.140(6)	0.165(7)	0.11(1)	-0.15(1)
	{5, 7}	0.385(6)	0.376(5)	0.373(5)	0.363(6)	0.34(1)	0.05(1)
	{7, 9}	0.568(3)	0.564(3)	0.563(3)	0.52(1)	0.538(8)	0.30(1)
	{9, 10.68}	0.686(1)	0.685(1)	0.685(1)	0.63(2)	0.674(3)	0.551(7)
$F_L^{\bar{B} \rightarrow D^* \tau^- \bar{\nu}}$	{3.157, 5}	0.61(1)	0.636(4)	0.643(5)	0.59(1)	0.648(5)	0.730(4)
	{5, 7}	0.500(9)	0.522(3)	0.528(4)	0.495(10)	0.534(5)	0.634(5)
	{7, 9}	0.411(5)	0.423(3)	0.427(3)	0.416(4)	0.433(4)	0.522(5)
	{9, 10.68}	0.357(2)	0.361(1)	0.363(2)	0.371(3)	0.365(2)	0.411(3)

TABLE XII: Predictions of various observables in the SM and different 1-operator scenarios for the  $\bar{B} \rightarrow D^* l \bar{\nu}$  channel.

- [22] A. Sibidanov *et al.* (Belle), Study of Exclusive  $B \rightarrow X_u \ell \nu$  Decays and Extraction of  $\|V_{ub}\|$  using Full Reconstruction Tagging at the Belle Experiment, Phys. Rev. D **88**, 032005 (2013), arXiv:1306.2781 [hep-ex].
- [23] J. A. Bailey *et al.* (MILC),  $B \rightarrow D \ell \nu$  form factors at nonzero recoil and  $-V_{cb}$  from 2+1-flavor lattice QCD, Phys. Rev. D **92**, 034506 (2015), arXiv:1503.07237 [hep-lat].
- [24] H. Na, C. M. Boucharad, G. P. Lepage, C. Monahan, and J. Shigemitsu (HPQCD),  $B \rightarrow D l \nu$  form factors at nonzero recoil and extraction of  $|V_{cb}|$ , Phys. Rev. D **92**, 054510 (2015), [Erratum: Phys.Rev.D 93, 119906 (2016)], arXiv:1505.03925 [hep-lat].

Obs	$q^2$ bins	$C_{V_1}, C_{V_2}$	$C_{V_1}, C_{S_1}$	$C_{V_1}, C_{S_2}$	$C_{V_1}, C_T$	$C_{V_2}, C_{S_1}$
$A_{FB}^{\bar{B} \rightarrow D\mu^- \bar{\nu}}$	{0.01, 2}	0.03325(5)	0.033(2)	0.033(2)	0.03325(6)	0.033(2)
	{2, 4}	0.00649(1)	0.006(3)	0.006(3)	0.00649(4)	0.006(3)
	{4, 6}	0.00423(1)	0.004(3)	0.004(3)	0.00423(5)	0.004(3)
	{6, 8}	0.00350(1)	0.003(4)	0.003(4)	0.00350(5)	0.003(4)
	{8, 10}	0.00348(1)	0.003(5)	0.003(5)	0.00348(6)	0.003(5)
	{10, 11.628}	0.00458(2)	0.004(7)	0.004(7)	0.0046(1)	0.004(7)
	<b>{0.01, 11.628}</b>	0.01381(8)	0.014(3)	0.014(3)	0.01380(9)	0.014(3)
$A_{\lambda_\ell}^{\bar{B} \rightarrow D\mu^- \bar{\nu}}$	{0.01, 2}	0.9106(1)	0.911(10)	0.911(10)	0.9106(1)	0.91(1)
	{2, 4}	0.98166(5)	0.98(1)	0.98(1)	0.98165(6)	0.98(1)
	{4, 6}	0.98722(5)	0.99(1)	0.99(2)	0.98722(6)	0.99(2)
	{6, 8}	0.98827(6)	0.99(2)	0.99(2)	0.98826(8)	0.99(2)
	{8, 10}	0.98581(9)	0.99(3)	0.99(3)	0.9858(1)	0.99(3)
	{10, 11.628}	0.9706(2)	0.98(8)	0.97(8)	0.9706(2)	0.98(8)
	<b>{0.01, 11.628}</b>	0.9615(2)	0.96(1)	0.96(2)	0.9615(2)	0.96(2)
$A_{FB}^{\bar{B} \rightarrow D\tau^- \bar{\nu}}$	{3.157, 5}	0.44315(8)	0.442(3)	-0.20(5)	0.445(4)	0.434(3)
	{5, 7}	0.39405(8)	0.393(3)	-0.36(1)	0.397(7)	0.383(4)
	{7, 9}	0.3494(2)	0.346(7)	-0.327(10)	0.35(1)	0.329(7)
	{9, 11.628}	0.2849(5)	0.28(2)	-0.19(1)	0.29(2)	0.24(1)
	<b>{3.157, 11.628}</b>	0.3600(2)	0.355(10)	-0.268(5)	0.365(10)	0.333(8)
$A_{\lambda_\ell}^{\bar{B} \rightarrow D\tau^- \bar{\nu}}$	{3.157, 5}	-0.314(2)	-0.34(4)	0.37(5)	-0.31(2)	-0.42(2)
	{5, 7}	-0.254(2)	-0.29(6)	0.02(9)	-0.25(1)	-0.40(3)
	{7, 9}	-0.277(3)	-0.32(8)	-0.44(7)	-0.27(2)	-0.47(4)
	{9, 11.628}	-0.496(3)	-0.54(8)	-0.81(3)	-0.49(1)	-0.68(3)
	<b>{3.157, 11.628}</b>	-0.323(3)	-0.36(7)	-0.48(6)	-0.32(2)	-0.50(4)

TABLE XIII: Predictions of various observables in different 2-operator scenarios in the  $\bar{B} \rightarrow D\ell\bar{\nu}$  channel. The rows with the  $q^2$ -bins written in bold font represent the predictions for the  $q^2$  integrated observables.

- [25] J. A. Bailey *et al.* (Fermilab Lattice, MILC), Update of  $|V_{cb}|$  from the  $\bar{B} \rightarrow D^*\ell\bar{\nu}$  form factor at zero recoil with three-flavor lattice QCD, Phys. Rev. D **89**, 114504 (2014), arXiv:1403.0635 [hep-lat].
- [26] J. A. Bailey *et al.* (Fermilab Lattice, MILC),  $B \rightarrow \pi\ell\ell$  form factors for new-physics searches from lattice QCD, Phys. Rev. Lett. **115**, 152002 (2015), arXiv:1507.01618 [hep-ph].
- [27] J. M. Flynn, T. Izubuchi, T. Kawanai, C. Lehner, A. Soni, R. S. Van de Water, and O. Witzel,  $B \rightarrow \pi\ell\nu$  and  $B_s \rightarrow K\ell\nu$  form factors and  $|V_{ub}|$  from 2+1-flavor lattice QCD with domain-wall light quarks and relativistic heavy quarks, Phys. Rev. D **91**, 074510 (2015), arXiv:1501.05373 [hep-lat].
- [28] A. Bazavov *et al.* (Fermilab Lattice, MILC), Semileptonic form factors for  $B \rightarrow D^*\ell\nu$  at nonzero recoil from 2 + 1-flavor lattice QCD, (2021), arXiv:2105.14019 [hep-lat].
- [29] B. Colquhoun, S. Hashimoto, T. Kaneko, and J. Koponen (JLQCD), Form factors of  $B \rightarrow \pi\ell\nu$  and a determination of  $|V_{ub}|$  with Möbius domain-wall-fermions, (2022), arXiv:2203.04938 [hep-lat].
- [30] Y. Aoki, B. Colquhoun, H. Fukaya, S. Hashimoto, T. Kaneko, R. Kellermann, J. Koponen, and E. Kou (JLQCD),  $B \rightarrow D^*\ell\nu_\ell$  semileptonic form factors from lattice QCD with Möbius domain-wall quarks, (2023), arXiv:2306.05657 [hep-lat].
- [31] Hflav fit results as of end of 22, [https://hflav-eos.web.cern.ch/hflav-eos/semi/fall122\\_fixed/html/RDsDsstar/RDRDs.html](https://hflav-eos.web.cern.ch/hflav-eos/semi/fall122_fixed/html/RDsDsstar/RDRDs.html) ().
- [32] Hflav fit results as of winter 23, [https://hflav-eos.web.cern.ch/hflav-eos/semi/winter23\\_prel/html/RDsDsstar/](https://hflav-eos.web.cern.ch/hflav-eos/semi/winter23_prel/html/RDsDsstar/)

Obs	$q^2$ bins	$C_{V_2}, C_{S_2}$	$C_{V_2}, C_T$	$C_{S_1}, C_T$	$C_{S_2}, C_T$	$C_{S_1}, C_{S_2}$
$A_{FB}^{\bar{B} \rightarrow D\mu^- \bar{\nu}}$	{0.01, 2}	0.033(2)	0.03325(6)	0.033(2)	0.033(2)	0.033(2)
	{2, 4}	0.006(3)	0.00649(4)	0.006(3)	0.006(3)	0.006(3)
	{4, 6}	0.004(3)	0.00423(5)	0.004(3)	0.004(3)	0.004(3)
	{6, 8}	0.003(4)	0.00350(5)	0.003(4)	0.003(4)	0.003(4)
	{8, 10}	0.003(5)	0.00348(6)	0.003(5)	0.003(5)	0.003(5)
	{10, 11.628}	0.005(7)	0.0046(1)	0.004(7)	0.004(7)	0.004(7)
	<b>{0.01, 11.628}</b>	0.014(3)	0.01381(9)	0.014(3)	0.014(3)	0.014(3)
$A_{\lambda_\ell}^{\bar{B} \rightarrow D\mu^- \bar{\nu}}$	{0.01, 2}	0.91(1)	0.9106(1)	0.911(10)	0.911(10)	0.911(10)
	{2, 4}	0.98(1)	0.98165(6)	0.98(1)	0.98(1)	0.98(1)
	{4, 6}	0.99(2)	0.98722(6)	0.99(1)	0.99(2)	0.99(1)
	{6, 8}	0.99(2)	0.98826(8)	0.99(2)	0.99(2)	0.99(2)
	{8, 10}	0.99(3)	0.9858(1)	0.99(3)	0.99(3)	0.99(3)
	{10, 11.628}	0.97(9)	0.9706(2)	0.98(8)	0.97(8)	0.98(8)
	<b>{0.01, 11.628}</b>	0.96(2)	0.9615(2)	0.96(1)	0.96(2)	0.96(2)
$A_{FB}^{\bar{B} \rightarrow D\tau^- \bar{\nu}}$	{3.157, 5}	-0.12(3)	0.430(3)	0.432(3)	-0.15(3)	0.439(3)
	{5, 7}	-0.33(2)	0.369(6)	0.377(5)	-0.35(1)	0.389(3)
	{7, 9}	-0.340(3)	0.311(9)	0.322(7)	-0.351(9)	0.340(6)
	{9, 11.628}	-0.212(8)	0.23(1)	0.24(1)	-0.22(1)	0.26(1)
	<b>{3.157, 11.628}</b>	-0.2725(2)	0.326(8)	0.329(8)	-0.285(8)	0.346(8)
$A_{\lambda_\ell}^{\bar{B} \rightarrow D\tau^- \bar{\nu}}$	{3.157, 5}	0.43(2)	-0.36(1)	-0.40(2)	0.41(2)	-0.37(3)
	{5, 7}	0.17(5)	-0.30(1)	-0.37(3)	0.12(5)	-0.34(4)
	{7, 9}	-0.31(5)	-0.33(1)	-0.43(4)	-0.34(5)	-0.39(5)
	{9, 11.628}	-0.75(2)	-0.541(10)	-0.64(4)	-0.76(2)	-0.61(5)
	<b>{3.157, 11.628}</b>	-0.37(4)	-0.37(1)	-0.46(4)	-0.40(4)	-0.43(5)

TABLE XIV: Predictions of various observables in different 2-operator scenarios in the  $\bar{B} \rightarrow D\ell\bar{\nu}$  channel. The rows with the  $q^2$ -bins written in bold font represent the predictions for the  $q^2$  integrated observables.

RDRDs.html ).

- [33] J. P. Lees *et al.* (BaBar), Evidence for an excess of  $\bar{B} \rightarrow D^{(*)}\tau^- \bar{\nu}_\tau$  decays, Phys. Rev. Lett. **109**, 101802 (2012), arXiv:1205.5442 [hep-ex].
- [34] J. P. Lees *et al.* (BaBar), Measurement of an Excess of  $\bar{B} \rightarrow D^{(*)}\tau^- \bar{\nu}_\tau$  Decays and Implications for Charged Higgs Bosons, Phys. Rev. D **88**, 072012 (2013), arXiv:1303.0571 [hep-ex].
- [35] M. Huschle *et al.* (Belle), Measurement of the branching ratio of  $\bar{B} \rightarrow D^{(*)}\tau^- \bar{\nu}_\tau$  relative to  $\bar{B} \rightarrow D^{(*)}\ell^- \bar{\nu}_\ell$  decays with hadronic tagging at Belle, Phys. Rev. D **92**, 072014 (2015), arXiv:1507.03233 [hep-ex].
- [36] G. Caria *et al.* (Belle), Measurement of  $\mathcal{R}(D)$  and  $\mathcal{R}(D^*)$  with a semileptonic tagging method, Phys. Rev. Lett. **124**, 161803 (2020), arXiv:1910.05864 [hep-ex].
- [37] R. Aaij *et al.* (LHCb), Measurement of the ratios of branching fractions  $\mathcal{R}(D^*)$  and  $\mathcal{R}(D^0)$ , (2023), arXiv:2302.02886 [hep-ex].
- [38] D. Bigi and P. Gambino, Revisiting  $B \rightarrow D\ell\nu$ , Phys. Rev. D **94**, 094008 (2016), arXiv:1606.08030 [hep-ph].
- [39] F. U. Bernlochner, Z. Ligeti, M. Papucci, and D. J. Robinson, Combined analysis of semileptonic  $B$  decays to  $D$  and  $D^*$ :  $R(D^{(*)})$ ,  $|V_{cb}|$ , and new physics, Phys. Rev. D **95**, 115008 (2017), [Erratum: Phys.Rev.D 97, 059902 (2018)], arXiv:1703.05330 [hep-ph].
- [40] S. Jaiswal, S. Nandi, and S. K. Patra, Extraction of  $|V_{cb}|$  from  $B \rightarrow D^{(*)}\ell\nu_\ell$  and the Standard Model predictions of  $R(D^{(*)})$ ,

Obs	$q^2$ bins	$C_{V_1}, C_{V_2}$	$C_{V_1}, C_{S_1}$	$C_{V_1}, C_{S_2}$	$C_{V_1}, C_T$	$C_{V_2}, C_{S_1}$
$A_{FB}^{\bar{B} \rightarrow D^* \mu^- \bar{\nu}}$	{0.01, 2}	-0.059(5)	-0.059(5)	-0.059(5)	-0.059(5)	-0.059(5)
	{2, 4}	-0.198(5)	-0.198(5)	-0.198(5)	-0.198(5)	-0.198(5)
	{4, 6}	-0.259(4)	-0.259(4)	-0.259(4)	-0.259(4)	-0.259(4)
	{6, 8}	-0.270(5)	-0.271(5)	-0.271(5)	-0.271(5)	-0.270(5)
	{8, 10}	-0.223(5)	-0.224(5)	-0.224(5)	-0.224(5)	-0.223(5)
	{10, 10.68}	-0.123(3)	-0.124(3)	-0.124(3)	-0.124(3)	-0.123(3)
	<b>{0.01, 10.68}</b>	-0.209(3)	-0.209(3)	-0.209(3)	-0.209(3)	-0.209(3)
$A_{\lambda_\ell}^{\bar{B} \rightarrow D^* \mu^- \bar{\nu}}$	{0.01, 2}	0.9276(5)	0.928(4)	0.927(4)	0.9276(9)	0.928(4)
	{2, 4}	0.9902(1)	0.990(3)	0.990(3)	0.9902(2)	0.990(3)
	{4, 6}	0.99552(5)	0.996(2)	0.995(2)	0.9955(1)	0.996(2)
	{6, 8}	0.99746(2)	0.9975(10)	0.997(1)	0.99746(8)	0.998(1)
	{8, 10}	0.998409(10)	0.9984(4)	0.9984(5)	0.99841(8)	0.9984(5)
	{10, 10.68}	0.998843(2)	0.9989(1)	0.9988(1)	0.99885(8)	0.9988(1)
	<b>{0.01, 10.68}</b>	0.9852(2)	0.985(2)	0.985(2)	0.9852(2)	0.985(2)
$F_L^{\bar{B} \rightarrow D^* \mu^- \bar{\nu}}$	{0.01, 2}	0.847(5)	0.848(5)	0.848(5)	0.848(5)	0.847(5)
	{2, 4}	0.636(5)	0.636(5)	0.636(5)	0.636(5)	0.636(5)
	{4, 6}	0.501(3)	0.501(3)	0.501(3)	0.501(3)	0.501(3)
	{6, 8}	0.415(3)	0.415(3)	0.415(3)	0.415(3)	0.415(3)
	{8, 10}	0.363(2)	0.363(2)	0.363(2)	0.363(2)	0.363(2)
	{10, 10.68}	0.3388(5)	0.3388(5)	0.3388(5)	0.3388(5)	0.3388(5)
	<b>{0.01, 10.68}</b>	0.530(3)	0.531(3)	0.531(3)	0.531(3)	0.530(3)
$A_{FB}^{\bar{B} \rightarrow D^* \tau^- \bar{\nu}}$	{3.157, 5}	0.122(10)	0.130(8)	0.218(4)	0.11(2)	0.158(9)
	{5, 7}	-0.01(1)	-0.005(9)	0.112(6)	-0.03(4)	0.03(1)
	{7, 9}	-0.10(1)	-0.091(8)	0.024(7)	-0.12(5)	-0.06(1)
	{9, 10.68}	-0.098(9)	-0.093(5)	-0.019(5)	-0.12(4)	-0.070(8)
	<b>{3.157, 10.68}</b>	-0.06(1)	-0.049(7)	0.059(6)	-0.07(4)	-0.018(10)
$A_{\lambda_\ell}^{\bar{B} \rightarrow D^* \tau^- \bar{\nu}}$	{3.157, 5}	0.145(6)	0.14(2)	-0.18(2)	0.14(2)	0.10(1)
	{5, 7}	0.376(5)	0.37(2)	0.02(2)	0.377(5)	0.34(1)
	{7, 9}	0.564(3)	0.56(1)	0.27(2)	0.57(2)	0.537(8)
	{9, 10.68}	0.685(1)	0.683(5)	0.54(1)	0.70(3)	0.674(3)
	<b>{3.157, 10.68}</b>	0.506(3)	0.50(1)	0.21(2)	0.51(1)	0.477(8)
$F_L^{\bar{B} \rightarrow D^* \tau^- \bar{\nu}}$	{3.157, 5}	0.634(5)	0.638(6)	0.738(6)	0.64(1)	0.655(5)
	{5, 7}	0.520(5)	0.525(7)	0.644(8)	0.527(9)	0.541(5)
	{7, 9}	0.422(4)	0.425(5)	0.532(8)	0.423(3)	0.437(4)
	{9, 10.68}	0.360(2)	0.362(2)	0.417(5)	0.356(10)	0.367(2)
	<b>{3.157, 10.68}</b>	0.452(4)	0.455(5)	0.561(7)	0.455(3)	0.468(4)

TABLE XV: Predictions of various observables in different 2-operator scenarios for the  $\bar{B} \rightarrow D^* l \bar{\nu}$  channel. The rows with the  $q^2$ -bins written in bold font represent the predictions for the  $q^2$  integrated observables.

Obs	$q^2$ bins	$C_{V_2}, C_{S_2}$	$C_{V_2}, C_T$	$C_{S_1}, C_T$	$C_{S_2}, C_T$	$C_{S_1}, C_{S_2}$
$A_{FB}^{\bar{B} \rightarrow D^* \mu^- \bar{\nu}}$	{0.01, 2}	-0.059(5)	-0.059(5)	-0.059(5)	-0.059(5)	-0.060(10)
	{2, 4}	-0.198(5)	-0.198(5)	-0.198(5)	-0.198(5)	-0.199(8)
	{4, 6}	-0.259(4)	-0.259(4)	-0.259(4)	-0.259(4)	-0.260(5)
	{6, 8}	-0.270(5)	-0.270(5)	-0.271(5)	-0.271(5)	-0.271(5)
	{8, 10}	-0.223(5)	-0.223(5)	-0.224(5)	-0.224(5)	-0.224(5)
	{10, 10.68}	-0.123(3)	-0.123(3)	-0.124(3)	-0.124(3)	-0.124(3)
	<b>{0.01, 10.68}</b>	-0.209(3)	-0.209(3)	-0.209(3)	-0.209(3)	-0.210(5)
$A_{\lambda_\ell}^{\bar{B} \rightarrow D^* \mu^- \bar{\nu}}$	{0.01, 2}	0.928(4)	0.9276(9)	0.928(4)	0.927(4)	0.93(3)
	{2, 4}	0.990(3)	0.9902(2)	0.990(3)	0.990(3)	0.99(2)
	{4, 6}	0.996(2)	0.9955(1)	0.996(2)	0.995(2)	0.997(8)
	{6, 8}	0.997(1)	0.99746(8)	0.9975(10)	0.997(1)	0.998(4)
	{8, 10}	0.9984(5)	0.99841(8)	0.9984(5)	0.9984(5)	0.999(1)
	{10, 10.68}	0.9988(1)	0.99885(8)	0.9989(1)	0.9988(1)	0.9989(2)
	<b>{0.01, 10.68}</b>	0.985(2)	0.9852(2)	0.985(2)	0.985(2)	0.99(1)
$F_L^{\bar{B} \rightarrow D^* \mu^- \bar{\nu}}$	{0.01, 2}	0.847(5)	0.847(5)	0.848(5)	0.848(5)	0.847(5)
	{2, 4}	0.636(5)	0.636(5)	0.636(5)	0.636(5)	0.636(5)
	{4, 6}	0.501(3)	0.501(3)	0.501(3)	0.501(3)	0.501(3)
	{6, 8}	0.415(3)	0.415(3)	0.415(3)	0.415(3)	0.415(3)
	{8, 10}	0.363(2)	0.363(2)	0.363(2)	0.363(2)	0.362(2)
	{10, 10.68}	0.3388(5)	0.3388(5)	0.3388(5)	0.3388(5)	0.3388(5)
	<b>{0.01, 10.68}</b>	0.530(3)	0.530(3)	0.531(3)	0.531(3)	0.530(3)
$A_{FB}^{\bar{B} \rightarrow D^* \tau^- \bar{\nu}}$	{3.157, 5}	0.205(6)	0.19(1)	0.17(1)	0.19(1)	0.20(1)
	{5, 7}	0.097(7)	0.08(2)	0.05(2)	0.07(2)	0.08(2)
	{7, 9}	0.007(8)	0.008(20)	-0.03(2)	-0.03(3)	-0.01(2)
	{9, 10.68}	-0.033(7)	0.004(19)	-0.04(2)	-0.08(4)	-0.04(1)
	<b>{3.157, 10.68}</b>	0.044(7)	0.04(2)	0.003(18)	0.01(3)	0.03(2)
$A_{\lambda_\ell}^{\bar{B} \rightarrow D^* \tau^- \bar{\nu}}$	{3.157, 5}	-0.18(2)	0.19(1)	0.13(2)	-0.20(3)	-0.07(6)
	{5, 7}	0.03(2)	0.34(2)	0.344(10)	0.02(3)	0.15(7)
	{7, 9}	0.27(2)	0.47(3)	0.52(1)	0.28(2)	0.38(6)
	{9, 10.68}	0.53(1)	0.55(4)	0.64(2)	0.564(9)	0.60(3)
	<b>{3.157, 10.68}</b>	0.21(2)	0.43(3)	0.47(1)	0.21(2)	0.32(6)
$F_L^{\bar{B} \rightarrow D^* \tau^- \bar{\nu}}$	{3.157, 5}	0.732(5)	0.52(4)	0.62(2)	0.750(8)	0.70(2)
	{5, 7}	0.638(7)	0.45(3)	0.51(1)	0.653(9)	0.60(2)
	{7, 9}	0.528(7)	0.40(1)	0.425(6)	0.534(7)	0.49(2)
	{9, 10.68}	0.416(5)	0.377(3)	0.372(3)	0.408(5)	0.39(1)
	<b>{3.157, 10.68}</b>	0.557(7)	0.42(1)	0.453(7)	0.564(8)	0.52(2)

TABLE XVI: Predictions of various observables in different 2-operator scenarios for the  $\bar{B} \rightarrow D^* l \bar{\nu}$  channel. The rows with the  $q^2$ -bins written in bold font represent the predictions for the  $q^2$  integrated observables.



Obs	$q^2$ bins	SM value	$C_{V_1}$	$C_{V_2}$	$C_T$	$C_{S_1}$	$C_{S_2}$
$A_{FB}^{\bar{B} \rightarrow \pi \mu^- \bar{\nu}}$	{0.01, 2}	0.0317±0.0002	0.0315±0.0001	0.0315±0.0001	0.0449±0.0123	0.0307±0.0081	0.0307±0.0081
	{2, 4}	0.00588±0.00004	0.00585±0.00003	0.00585±0.00003	0.02049±0.01324	0.00497±0.00892	0.00497±0.00892
	{4, 6}	0.00351±0.00004	0.00348±0.00003	0.00348±0.00003	0.01832±0.01323	0.00259±0.00912	0.00259±0.00912
	{6, 8}	0.00254±0.00004	0.00252±0.00003	0.00252±0.00003	0.01752±0.01319	0.00160±0.00930	0.00160±0.00930
	{8, 10}	0.00201±0.00003	0.00199±0.00003	0.00199±0.00003	0.01719±0.01317	0.00106±0.00952	0.00106±0.00952
	{10, 12}	0.00169±0.00003	0.00167±0.00003	0.00167±0.00003	0.01713±0.013176	0.00071±0.00978	0.00071±0.00978
	{12, 14}	0.00147±0.00003	0.00146±0.00003	0.00146±0.00003	0.01727±0.01325	0.00047±0.01011	0.00047±0.01011
	{14, 16}	0.00133±0.00003	0.00132±0.00003	0.00132±0.00003	0.01761±0.01343	0.00029±0.01054	0.00029±0.01054
	{16, 18}	0.00124±0.00003	0.00123±0.00003	0.00123±0.00003	0.01822±0.01376	0.00014±0.01112	0.00014±0.01112
	{18, 20}	0.00118±0.00003	0.00118±0.00003	0.00118±0.00003	0.01921±0.01435	0.000009±0.011934	0.000009±0.011934
	{20, 22}	0.00118±0.00003	0.001178±0.00003	0.001178±0.00003	0.02086±0.01539	-0.00011±0.01316	-0.00011±0.01316
	{22, 24}	0.00125±0.00003	0.00125±0.00003	0.00125±0.00003	0.02386±0.01740	-0.00025±0.01524	-0.00025±0.01524
	{24, 26.4}	0.00154±0.00004	0.00154±0.00004	0.00154±0.00004	0.03172±0.02283	-0.00046±0.02040	-0.00046±0.02040
	$A_{\lambda_\ell}^{\bar{B} \rightarrow \pi \mu^- \bar{\nu}}$	{0.01, 2}	0.9151±0.0006	0.9157±0.0003	0.9157±0.0003	0.8901±0.0320	0.9188±0.0313
{2, 4}		0.9842±0.0002	0.9843±0.0001	0.9843±0.0001	0.9386±0.0670	0.9876±0.0306	0.9876±0.0306
{4, 6}		0.9905±0.0002	0.9906±0.0001	0.9906±0.0001	0.9272±0.0992	0.9938±0.0278	0.9938±0.0278
{6, 8}		0.9930±0.0002	0.9931±0.0001	0.9931±0.0001	0.9126±0.1301	0.9963±0.0247	0.9963±0.0247
{8, 10}		0.9944±0.0001	0.9945±0.0001	0.9945±0.0001	0.8973±0.1599	0.9975±0.0216	0.9975±0.0216
{10, 12}		0.9952±0.0001	0.9953±0.0001	0.9953±0.0001	0.8820±0.1884	0.9983±0.0182	0.9983±0.0182
{12, 14}		0.9958±0.0001	0.9958±0.0001	0.9958±0.0001	0.8669±0.2157	0.9988±0.0147	0.9988±0.0147
{14, 16}		0.9961±0.0001	0.9961±0.0001	0.9961±0.0001	0.8521±0.2415	0.9991±0.0107	0.9991±0.0107
{16, 18}		0.9962±0.0001	0.9963±0.0001	0.9963±0.0001	0.8377±0.2660	0.9993±0.0061	0.9993±0.0061
{18, 20}		0.9962±0.0002	0.9962±0.0002	0.9962±0.0002	0.8236±0.2891	0.9994±0.0004	0.9994±0.0004
{20, 22}		0.9960±0.0002	0.9960±0.0002	0.9960±0.0002	0.8096±0.3109	0.9994±0.0077	0.9994±0.0077
{22, 24}		0.9952±0.0002	0.9952±0.0002	0.9952±0.0002	0.7953±0.3320	0.9993±0.0212	0.9993±0.0212
{24, 26.4}		0.9922±0.0004	0.9922±0.0004	0.9922±0.0004	0.7783±0.3529	0.9988±0.0601	0.9988±0.0601

TABLE XVII: Predictions of various observables in the SM and different new physics scenarios for the  $\bar{B} \rightarrow \pi l \bar{\nu}$  channel using the fit results of the left column of table IX for the scenarios with  $\mathcal{O}_T$ ,  $\mathcal{O}_{S_1}$ ,  $\mathcal{O}_{S_2}$  and the right column for the scenarios with  $\mathcal{O}_{V_1}$ ,  $\mathcal{O}_{V_2}$ .

JHEP **12**, 060, arXiv:1707.09977 [hep-ph].

- [41] M. Bordone, M. Jung, and D. van Dyk, Theory determination of  $\bar{B} \rightarrow D^{(*)} \ell^- \bar{\nu}$  form factors at  $\mathcal{O}(1/m_c^2)$ , Eur. Phys. J. C **80**, 74 (2020), arXiv:1908.09398 [hep-ph].
- [42] S. Hirose *et al.* (Belle), Measurement of the  $\tau$  lepton polarization and  $R(D^*)$  in the decay  $\bar{B} \rightarrow D^* \tau^- \bar{\nu}_\tau$  with one-prong hadronic  $\tau$  decays at Belle, Phys. Rev. D **97**, 012004 (2018), arXiv:1709.00129 [hep-ex].
- [43] R. Aaij *et al.* (LHCb), Test of lepton flavour universality using  $B^0 \rightarrow D^{*-} \tau^+ \nu_\tau$  decays with hadronic  $\tau$  channels, (2023), arXiv:2305.01463 [hep-ex].
- [44] R. Aaij *et al.* (LHCb), Test of Lepton Flavor Universality by the measurement of the  $B^0 \rightarrow D^{*-} \tau^+ \nu_\tau$  branching fraction using three-prong  $\tau$  decays, Phys. Rev. D **97**, 072013 (2018), arXiv:1711.02505 [hep-ex].
- [45] J. P. Lees *et al.* (BaBar), Extraction of form Factors from a Four-Dimensional Angular Analysis of  $\bar{B} \rightarrow D^* \ell^- \bar{\nu}_\ell$ , Phys. Rev. Lett. **123**, 091801 (2019), arXiv:1903.10002 [hep-ex].
- [46] A. Abdesselam *et al.* (Belle), Measurement of the  $D^{*-}$  polarization in the decay  $B^0 \rightarrow D^{*-} \tau^+ \nu_\tau$ , *10th International Workshop on the CKM Unitarity Triangle*, (2019), arXiv:1903.03102 [hep-ex].
- [47] S. Bhattacharya, S. Nandi, and S. Kumar Patra,  $b \rightarrow c \tau \nu_\tau$  Decays: a catalogue to compare, constrain, and correlate new physics effects, Eur. Phys. J. **C79**, 268 (2019), arXiv:1805.08222 [hep-ph].
- [48] Z.-R. Huang, Y. Li, C.-D. Lu, M. A. Paracha, and C. Wang, Footprints of New Physics in  $b \rightarrow c \tau \nu$  Transitions, Phys. Rev. D **98**, 095018 (2018), arXiv:1808.03565 [hep-ph].
- [49] B. Henning, X. Lu, and H. Murayama, How to use the Standard Model effective field theory, JHEP **01**, 023, arXiv:1412.1837 [hep-ph].
- [50] E. E. Jenkins, A. V. Manohar, and P. Stoffer, Low-Energy Effective Field Theory below the Electroweak Scale: Operators and Matching, JHEP **03**, 016, arXiv:1709.04486 [hep-ph].
- [51] J. Aebischer, A. Crivellin, M. Fael, and C. Greub, Matching of gauge invariant dimension-six operators for  $b \rightarrow s$  and

- $b \rightarrow c$  transitions, JHEP **05**, 037, arXiv:1512.02830 [hep-ph].
- [52] Y. Sakaki, M. Tanaka, A. Tayduganov, and R. Watanabe, Testing leptoquark models in  $\bar{B} \rightarrow D^{(*)}\tau\bar{\nu}$ , Phys. Rev. D **88**, 094012 (2013), arXiv:1309.0301 [hep-ph].
- [53] D. Bigi, P. Gambino, and S. Schacht,  $R(D^*)$ ,  $|V_{cb}|$ , and the Heavy Quark Symmetry relations between form factors, JHEP **11**, 061, arXiv:1707.09509 [hep-ph].
- [54] C. G. Boyd, B. Grinstein, and R. F. Lebed, Constraints on form factors for exclusive semileptonic heavy to light meson decays, Phys. Rev. Lett. **74**, 4603 (1995).
- [55] C. G. Boyd, B. Grinstein, and R. F. Lebed, Precision corrections to dispersive bounds on form-factors, Phys. Rev. **D56**, 6895 (1997), arXiv:hep-ph/9705252 [hep-ph].
- [56] D. Bečirević, M. Fedele, I. Nišandžić, and A. Tayduganov, Lepton Flavor Universality tests through angular observables of  $\bar{B} \rightarrow D^{(*)}\ell\bar{\nu}$  decay modes, (2019), arXiv:1907.02257 [hep-ph].
- [57] A. Bharucha, D. M. Straub, and R. Zwicky,  $B \rightarrow V\ell^+\ell^-$  in the Standard Model from light-cone sum rules, JHEP **08**, 098, arXiv:1503.05534 [hep-ph].
- [58] C. Bourrely, I. Caprini, and L. Lellouch, Model-independent description of  $B \rightarrow \pi l \nu$  decays and a determination of  $-V(\text{ub})-$ , Phys. Rev. D **79**, 013008 (2009), [Erratum: Phys.Rev.D 82, 099902 (2010)], arXiv:0807.2722 [hep-ph].
- [59] N. Gubernari, A. Kokulu, and D. van Dyk,  $B \rightarrow P$  and  $B \rightarrow V$  Form Factors from  $B$ -Meson Light-Cone Sum Rules beyond Leading Twist, JHEP **01**, 150, arXiv:1811.00983 [hep-ph].
- [60] Ckmfitter global fit results as of summer 19, [http://ckmfitter.in2p3.fr/www/results/plots\\_spring21/num/ckmEval\\_results\\_spring21.html](http://ckmfitter.in2p3.fr/www/results/plots_spring21/num/ckmEval_results_spring21.html).
- [61] M. Blanke, A. Crivellin, S. de Boer, T. Kitahara, M. Moscati, U. Nierste, and I. Nišandžić, Impact of polarization observables and  $B_c \rightarrow \tau\nu$  on new physics explanations of the  $b \rightarrow c\tau\nu$  anomaly, Phys. Rev. D **99**, 075006 (2019), arXiv:1811.09603 [hep-ph].
- [62] D. Bardhan and D. Ghosh,  $B$ -meson charged current anomalies: The post-Moriond 2019 status, Phys. Rev. D **100**, 011701 (2019), arXiv:1904.10432 [hep-ph].
- [63] M. Fedele, M. Blanke, A. Crivellin, S. Iguro, T. Kitahara, U. Nierste, and R. Watanabe, Impact of  $\Lambda b \rightarrow \Lambda c\tau\nu$  measurement on new physics in  $b \rightarrow c\ell\nu$  transitions, Phys. Rev. D **107**, 055005 (2023), arXiv:2211.14172 [hep-ph].
- [64] R. Alonso, B. Grinstein, and J. Martin Camalich, Lifetime of  $B_c^-$  Constrains Explanations for Anomalies in  $B \rightarrow D^{(*)}\tau\nu$ , Phys. Rev. Lett. **118**, 081802 (2017), arXiv:1611.06676 [hep-ph].
- [65] A. Biswas and S. Nandi, A closer look at observables from exclusive semileptonic  $B \rightarrow (\pi, \rho)\ell\nu_\ell$  decays, JHEP **09**, 127, arXiv:2105.01732 [hep-ph].
- [66] R. Alonso, E. E. Jenkins, A. V. Manohar, and M. Trott, Renormalization Group Evolution of the Standard Model Dimension Six Operators III: Gauge Coupling Dependence and Phenomenology, JHEP **04**, 159, arXiv:1312.2014 [hep-ph].
- [67] M. González-Alonso, J. Martin Camalich, and K. Mimouni, Renormalization-group evolution of new physics contributions to (semi)leptonic meson decays, Phys. Lett. B **772**, 777 (2017), arXiv:1706.00410 [hep-ph].
- [68] F. Feruglio, P. Paradisi, and O. Sumensari, Implications of scalar and tensor explanations of  $R_{D^{(*)}}$ , JHEP **11**, 191, arXiv:1806.10155 [hep-ph].
- [69] E. E. Jenkins, A. V. Manohar, and M. Trott, Renormalization Group Evolution of the Standard Model Dimension Six Operators II: Yukawa Dependence, JHEP **01**, 035, arXiv:1310.4838 [hep-ph].
- [70] D. Gonçalves, T. Han, and S. Mukhopadhyay, Higgs Couplings at High Scales, Phys. Rev. D **98**, 015023 (2018), arXiv:1803.09751 [hep-ph].
- [71] S. Iguro, T. Kitahara, Y. Omura, R. Watanabe, and K. Yamamoto,  $D^*$  polarization vs.  $R_{D^{(*)}}$  anomalies in the leptoquark models, JHEP **02**, 194, arXiv:1811.08899 [hep-ph].